Changes in total Ocean mass derived from GRACE, GPS, and Ocean Modelling with weekly Resolution

R. Rietbroek,[1,3] S.-E. Brunnabend,[2] Ch. Dahle,[1] J. Kusche,[1,3] F. Flechtner,[1] J. Schröter,[2] R. Timmermann[2]

Abstract. We derive changes in ocean bottom pressure and ocean mass by combining modelled ocean bottom pressure, weekly GRACE-derived models of gravity change, and large-scale deformation patterns sensed by a global network of GPS stations in a joint least-squares inversion. The weekly combination allows a consistent estimation of geocenter motion, loading mass harmonics up to degree 30, and a spatially uniform mass correction term, which serves as a correction for forcing of the ocean model. We provide maps and time series of ocean mass and bottom pressure variations. Furthermore, we discuss the estimated geocenter motion and the estimated model correction. Our results indicate that the total ocean mass change is predominantly annual, with a maximum amplitude corresponding to 7.4 mm in October, which is in line with earlier work. The mean ocean bottom pressure (i.e. ocean plus atmospheric mass) shows an annual amplitude of 8.7 mm and is shifted forward by about 1.5 months. In addition, the solution exhibits typical autocorrelation times of about 2 weeks. A comparison with in situ bottom pressure time series in the Southern Indian Ocean shows a good agreement, with correlations of 0.7-0.8. Based on these comparisons, we see that our results monitor realistic submonthly variations, which are strongest at high latitudes. The addition of GRACE data in the inversion is found to improve these high latitude variations and enables better separability of the geocenter motion from other unknowns. Increasing the OBP model error from 3 cm to 4.8 cm affects mainly the higher degree coefficients.

1. Introduction

The mass budget of the ocean is a key problem in quantifying the global hydrological cycle as well as in our understanding of sea level change. Spatial variability of ocean mass is dominated by the redistribution of water related to ocean circulation. On the other hand, changes in the total ocean mass exist due to the predominantly seasonal cycles of river runoff, evaporation/precipitation, and ice sheet thawing. Space-geodetic observations (time-variable gravity, altimetry) have confirmed this (see *Chambers et al.* [2004]; *Wu et al.* [2006]; *Willis et al.* [2008] and the references provided therein). They indicate that the seasonal variability of mass amounts to 6-8 mm water level when distributed evenly over the ocean, peaking in September - October, and that interannual variations occur.

However, variations in ocean mass on timescales longer and shorter than the annual period are significantly less well observed with geodetic tools. Its extraction from hydrological, oceanic and atmospheric models is even more difficult since these suffer in general from mass inconsistencies.

Short-period, non-tidal, temporal mass variability in the ocean has been studied by some authors in the context of de-aliasing satellite-altimetric (*Stammer et al.* [2000]) or satellite-gravimetric (*Thompson et al.* [2004]; *Dobslaw and Thomas* [2007]) observations. High-frequency (with period shorter than 10 days), predominantly barotropic motions in the ocean, when referenced to monthly means, were shown to cause pressure variability of up to 10 hPa (*Dobslaw and Thomas* [2007]) or geoid variability of up to 2 mm (*Thompson et al.* [2004]).

At this point, it becomes necessary to distinguish between ocean mass change and ocean bottom pressure change (OBP). The change in ocean mass is related to ocean surface fluxes and river runoff and is observed, when corrected for steric changes, and the smaller deformations of the ocean floor, by satellite altimetry. These deformations are caused by the response of the solid Earth which deforms (elastically) under the changing global surface load (*Farrell* [1972]). In contrast, the ocean bottom pressure change reflects also atmospheric mass variations, it may be predicted by general ocean circulation models, forced by atmospheric winds and pressure, and can also be observed by satellite gravity missions, such as GRACE.

Atmospheric surface pressure adds significant short-term variability to the (vertically integrated) column of oceanic and atmospheric masses. Due to the exchange of atmospheric masses across the coast, the spatial average of the atmospheric surface pressure over the ocean does not vanish and contains short-term variability. The total ocean mass content however is unaffected by changes in mean surface pressure since it does not induce a land-ocean exchange of water. On the other hand, changes in the mean atmospheric pressure may slightly affect the mean geocentric sea level, as observed by altimetry, as it can result in a net ocean floor deformation. The magnitude of this effect is small however. Under the assumption of a perfect IB response over the ocean (the ocean surface is loaded with a uniform pressure) and using the atmospheric GRACE GAA product, we found an annual amplitude of the mean deformation of

[1] GFZ German Research Centre for Geosciences, Potsdam, Germany.
[2] Alfred-Wegener-Institut Bremerhaven, Germany.
[3] Institute of Geodesy and Geoinformation, Bonn, Germany.

0148-0227/09/$9.00

0.4 mm.

Using satellite gravimetry to monitor ocean mass changes through their associated gravity and geoid effect requires a number of non-trivial issues to be taken into account (*Chambers et al.* [2004]; *Chambers* [2006]; *Ponte et al.* [2007]). These constitute of missing degree-1 coefficients, the treatment of ill-determined degree-2 coefficients, the correct restitution of the background ocean model, the ocean pole tide correction and dedicated filter techniques for the Stokes coefficients (e.g.*Swenson and Wahr* [2006]; *Kusche* [2007]). For example, *Chambers et al.* [2007] have shown by simulations that errors introduced by not accounting for secular motion of the geocenter (degree-1 terms) can be as large as 30-50 % of the recovered sea level (mass) trend. This secular geocenter trend, however, is relatively uncertain as determined from space-geodetic measurements. Furthermore, a comparison of the GRACE solution from the Centre for Space Research (CSR) and that from the German GeoForschungsZentrum (GFZ) showed a difference in trends of total ocean mass. This discrepancy has been suspected to originate in aliasing of mismodelled K2 tides (*Willis et al.* [2008]). Since the first GRACE release, the degree 2 coefficients have become increasingly more accurate, although the C_{20} coefficients are still affected by S2 tidal aliasing at the 161 day period *Chen and Wilson* [2008]; *Chen et al.* [2008].

The retrieval of ocean mass variations by Satellite altimetry (*Chambers et al.* [2004]) and oceanographic modelling (*Wenzel and Schröter* [2007]) is possible, but again, several important issues must be handled: Most notably, geocentric sea level change needs to be corrected for steric expansion of the water volume, adding a significant source of uncertainty. Moreover, satellite altimeters do not cover high latitudes and hypothesis must be made about mass change beyond the reach of the altimeters. Oceanographic modelling, even if mass-conservation is strived for, suffers from input uncertainties in the surface fluxes and river runoff.

Blewitt and Clarke [2003] introduced the technique of GPS loading inversion to weigh the changing mass of the ocean (and the atmosphere) by measuring its associated elastic deformation effect. The used GPS ground station network allows for a high temporal resolution and is less sensitive to orbit geometries. Unfortunately, the density and heterogeneity of the high-quality sites limits the achievable spatial resolution of global estimates to several thousands of km.

Here we will base our investigation on a statistically optimal combination of three techniques: 1) measuring time-variable gravity, 2) ocean modelling and 3) monitoring of the geometric deformation. In earlier studies joint estimates have been produced by combining data from GRACE, GPS and ocean bottom pressure from ECCO (Estimating the Circulation & Climate of the Ocean) in various combinations. A combination of GRACE+GPS was produced by *Kusche and Schrama* [2005] while a GRACE+GPS+ECCO inversion has been demonstrated by *Wu et al.* [2006].

The combination allows, to a large extent, the compensation of individual weaknesses of the techniques by the strengths of the other (cf. *Jansen et al.* [2009], for a formal analysis). This was first suggested by *Wu et al.* [2006], in conjunction with the estimation of a spatially homogeneous ocean model mass correction. In a joint estimation the issues, as pointed out by *Quinn and Ponte* [2008], can be adequately addressed. The mass conservation of the ocean model can be constrained, the accuracy of geocenter motion will increase, and the realistic higher resolution information of the ocean model is kept.

Specifically, in this work GRACE data, as well as GPS and modelled OBP, have weekly resolution and are aligned with the GPS calendar. This allows us to monitor ocean mass changes at weekly resolution for the first time. In addition, we investigate what the effect of different data weighting in this complex inverse problem is. The modelling of sea-ice interactions within the ocean model, resolving OBP changes also in polar regions, allows for an investigation of the effects of the common latitude-restriction seen in other models. Finally, the covariances obtained from the joint estimates will be used to investigate how important parameters, such as low degree coefficients and geocenter motion, correlate and can be separated from each other.

2. Methods

The three data sets that we use in this study represent globally distributed measurements, although they do not cover the Earth homogeneously. Nevertheless, we base our inversion on an expansion of the change in total surface (vertically integrated) loading mass density in spherical harmonics, as suggested originally in *Wahr et al.* [1998]:

$$\Delta\sigma(\lambda,\theta,t) = a\rho_w \sum_{n=1}^{N} \sum_{m=-n}^{n} T^{\sigma}_{nm}(t)\bar{Y}_{nm}(\lambda,\theta) \tag{1}$$

Where the fully normalised spherical harmonic base functions contain the associated Legendre functions, $\bar{P}_{nm}$, and are defined by:

$$\bar{Y}_{nm}(\lambda,\theta) = \begin{cases} \bar{P}_{n|m|}(\cos\theta)\cos m\lambda, & m \geq 0 \\ \bar{P}_{n|m|}(\cos\theta)\sin m\lambda, & m < 0 \end{cases}$$

Here $\Delta\sigma(\lambda,\theta,t) = \sigma(\lambda,\theta,t) - \sigma_0(\lambda,\theta)$ is the surface mass density function (expressed in $^{\mathrm{kg}}/_{\mathrm{m}^2}$) relative to a reference state, a is the mean Earth radius, ρ_w the mean density of sea water (assumed to 1025 $^{\mathrm{kg}}/_{\mathrm{m}^3}$). The benefit of employing spherical harmonics is in the fact that they allow for conservation of mass in the solutions (by setting T^{σ}_{00} to zero), that they allow control over the maximum surface resolution that can be fit to the data (through the choice of N), and that they represent eigenfunctions of surface loading phenomena in symmetric, non-rotating isotropic elastic Earth (SNREI) models.

The time-dependent coefficients T^{σ}_{nm}, $n, |m| \leq N$, represent a solution of the problem. Once determined, they can be used to retrieve the total ocean/atmospheric mass change expressed in equivalent water height, ΔM, by spectrally 'windowing' over the ocean area:

$$\Delta M = \frac{a}{O_{00}w_0} \sum_{n=1}^{N} \sum_{m=-n}^{n} T^{\sigma}_{nm}(t) O_{nm} w_n \tag{2}$$

Where O_{nm} are the spherical harmonic coefficients of the ocean function $O(\lambda,\theta)$, and w_n are the spectral coefficients of a suitable degree dependent weight function (In this study we used a spectral kernel derived from a Gaussian with 300 km halfwidth).

In our inversion scheme, three preprocessed data sets are considered: GRACE spherical harmonic coefficients of geopotential change with full covariance information, geometric station displacements derived from the IGS-GPS network, and ocean bottom pressure values produced by modelling. They are all weekly temporal averages, aligned to the

GPS calendar and are combined per week without considering temporal correlations. We seek a solution that fits all three data sets in an optimal weighted least-squares sense, by minimising the quadratic cost functional $\mathcal{L}_{\kappa,\beta,\gamma}$:

$$\begin{aligned}\mathcal{L}_{\kappa,\beta,\gamma} &= \kappa||\mathbf{y}_{\mathrm{GPS}} - \mathbf{Ax}||_{\mathbf{C}^{-1}_{\mathrm{GPS}}} + \beta||\mathbf{y}_{\mathrm{GRC}} - \mathbf{Bx}||_{\mathbf{C}^{-1}_{\mathrm{GRC}}} \\ &+ \gamma||\mathbf{y}_{\mathrm{OBP-MOD}} - \mathbf{Hx}||_{\mathbf{C}^{-1}_{\mathrm{OBP-MOD}}}\end{aligned} \quad (3)$$

Each vector of observations is represented by $\mathbf{y}_{\mathrm{type}}$, with the subscript denoting its type. In constructing data residuals, we use the design matrices, $\mathbf{A}, \mathbf{B}, \mathbf{H}$, which linearly propagate the solution vector, $\mathbf{x}$, in the observational domain. The functional penalizes the observation residual, which is weighted by its covariance information, $\mathbf{C}_{\mathrm{type}}$. Additionally, we may strengthen or weaken the influence of the each observation set by introducing the artificial weights, κ, β, γ. The solution vector contains the variables we do not consider as error free:

$$\mathbf{x} = \begin{pmatrix} T^{\sigma}_{nm} \quad n > 1 \\ \vec{\mathbf{G}}_{CE-CM} = \frac{\vec{\mathbf{m}}}{M_E} \\ \Delta M_0 \\ \delta\vec{\tau}, \delta\vec{\epsilon}, \delta s \end{pmatrix} \quad (4)$$

The degree 1 component of the T^{σ}_{nm} coefficients are represented in the load moment vector, $\vec{\mathbf{m}}$, which is virtually independent on the choice of terrestrial frame, scaled by the reciprocal mass of the solid Earth, M_E. This rescaled moment vector can be conveniently interpreted as the 'geocenter' motion i.e. the geometric offset of the center of mass of the solid Earth (CE) referred to the center of mass of the solid Earth - ocean - atmosphere - hydrosphere system (CM) (e.g. *Kusche and Schrama* [2005]). Furthermore, since the relative displacements of the CE and CF (center of figure of the Solid Earth) frame coincide to about 2 %, the values also closely approximate the motion of the CF frame with respect to the center of common mass of the Earth (*Blewitt and Clarke* [2003]). By applying the isomorphic frame transformations of *Blewitt and Clarke* [2003] one can express the solution in a reference frame of choice.

The parameter space of the inversion includes other elements such as a mass correction ΔM_0 of the OBP grid values (necessary due to inaccuracies in modelling freshwater fluxes), assumed as spatially uniform (*Wu et al.* [2006]), and a residual reference frame translation s $\delta\vec{\tau}$, rotation $\delta\vec{\epsilon}$ and scaling δs possibly affecting our geometric observations.

Our optimization functional, eq. 3, is stated in a rather general form for the sake of discussion here. Usually, with $\kappa, \beta, \gamma > 0$, we perform a weighted GPS-GRACE-OBP inversion, as suggested in *Wu et al.* [2006]. The main results shown in section 4 of this paper are produced in this way. Additionally we produced a GPS-OBP combination by setting $\kappa, \gamma > 0$, $\beta = 0$. However, to put our method in the broader context, other choices of these 'switches' shall be discussed briefly.

GPS-only inversion ($\kappa = 1, \beta = \gamma = 0$) was suggested by *Blewitt and Clarke* [2003] for weighing the total ocean mass change (in fact, as a preprocessing to our joint data inversion we perform such an inversion for detecting outliers in the station displacement data set). This technique has to cope with spatial truncation and associated aliasing effects. Even if one is aiming solely at the geocenter terms, some authors (e.g. *Munekane* [2007]) have suggested to implement GRACE-derived load estimates for degrees $n > 1$ to absorb spatial aliasing signal (that is, $\kappa = 1, \beta \gg 1, \gamma = 0$ in the above scheme). *Munekane* [2007] found the residual scaling parameter δs (see eq. 4) significantly reduced by using GRACE, as compared to GPS-only inversion for the geocenter terms. In the same spirit, one could use instead OBP model values for spatial de-aliasing ($\kappa = 1, \beta = 0, \gamma \gg 1$) which would be an improved version of the 'ocean regularization' method by *Kusche and Schrama* [2005]. Finally, the setting ($\kappa = 0, \beta > 0, \gamma > 0$), combines modelled OBP and GRACE-derived surface loading estimates to produce estimates of the geocenter terms (*Jansen et al.* [2009]).

Satellite-gravimetric and geometric observations sense redistributions of mass in ocean, atmosphere and terrestrial water storage systems, which are in principle inseparable. Atmospheric mass change fields provided by the ECMWF or NCEP centres are not error-free at the level of accuracy that we are interested in (*Salstein et al.* [2008]). We therefore decided neither to remove the atmospheric contribution from the observations nor from the modelled OBP values prior to the inversion but rather solve for the total contribution (best-fitting OBP spherical harmonic expansion). Then, the atmospheric contribution can be subtracted afterwards to obtain a spatial representation of the ocean mass redistribution.

2.1. Observation equations

In this study we consider three observables which can be linked to the surface density distribution of eq. 1. These are 1) changes in the external potential of the Earth, 2) 3-D geometrical deformation of the crust 3) changes in pressure at the ocean floor. While pressure changes depend only on the direct distribution of surface density, a geometrical deformation of the Earth under this load only occurs when we assume a non-rigid Earth. Combined, the surface density and its associated deformation will contribute to the gravity changes as measured by GRACE.

2.1.1. Gravity change

External temporal and spatial variations of gravity, induced by the surface loading, are measured by various spaceborne techniques. These include GRACE satellite to satellite tracking, CHAMP high-low tracking, and in the near future GOCE gradiometry. Usually the Stokes coefficients of the Earth are estimated up to a certain degree, implying that a certain smoothness of the solution is postulated. The temporally varying spherical harmonic coefficients of the geopotential field can be referred to surface mass change by assuming that all relevant changes take place within a thin layer at the surface of the Earth (*Wahr et al.* [1998]). Although this assumption is close to reality, it does require that all other mass signals can be removed (i.e. post-glacial rebound, plate motion).

As the Earth reacts with an 'indirect' potential to loading (the potential change due to the deformation of the Earth), an Earth model has to be implemented, typically involving load Love numbers k'_n. In the spectral domain, a simple one-to-one mapping between spherical coefficients of geopotential change, $\delta\Phi_{nm}$, and mass change is then possible:

$$\delta\Phi_{nm}(t) = \frac{3\rho_w(1 + k'_n)}{\rho_e(2n + 1)} T^{\sigma}_{nm}(t) \quad (5)$$

Where, ρ_e, is the mean density of the Earth.

2.1.2. Geometric change

As the Earth is not rigid, mass redistribution in atmosphere, ocean and on the continents leads to a deformation of the surface. Geometric positioning techniques like GPS, SLR and VLBI, can be used to observe this deformation, having orders up to a centimeter. On the other hand, at the time scales considered here, elastic loading theories (involving load Love and Shida numbers h'_n and l'_n) are fairly accurate in predicting such deformation of the crust if the loading mass distribution is known. Consequently, one may identify and invert large-scale pattern of station displacements from the solutions of global GPS networks into models of loading mass. This was done by *Blewitt and Clarke* [2003] on a global scale and by *Davis et al.* [2004] for the Amazon region.

Implementing elastic loading theory requires that in the time series of station displacements any real motion that is not caused by elastic loading (tectonics, Earthquakes, postglacial rebound) is absent or removed. Similarly, virtual motion due to antenna changes, snow coverage of the antenna, signal propagation effects should be ruled out. Then, loading inversion is usually performed through spherical harmonic expansion either from vertical motion only, or from vertical and horizontal displacements by imposing the Love-Shida hypothesis.

The spheroidal part of the observed geometric displacement in the up, east and north direction, $\delta h, \delta e, \delta n$, can be related to the solution vector by (*Kusche and Schrama* [2005]):

$$
\begin{aligned}
\delta h(\lambda,\theta,t) &= h'_1 \vec{\mathbf{G}}_{CE-CM}\cdot\vec{\mathbf{e}}_{\mathbf{h}} + \delta\vec{\tau}\cdot\vec{e}_h - a\delta s \\
&+ \frac{3a\rho_w}{\rho_e}\sum_{n=2}^{N}\sum_{m=-n}^{n}\frac{h'_n}{2n+1}T^{\sigma}_{nm}(t)\bar{Y}_{nm}(\lambda,\theta) \\
\delta e(\lambda,\theta,t) &= l'_1 \vec{\mathbf{G}}_{CE-CM}\cdot\vec{\mathbf{e}}_{\mathbf{e}} + \delta\vec{\tau}\cdot\vec{\mathbf{e}}_{\mathbf{e}} + \delta\vec{\epsilon}\cdot\vec{\mathbf{e}}_{\mathbf{n}} \\
&+ \frac{3a\rho_w}{\rho_e\sin\theta}\sum_{n=2}^{N}\sum_{m=-n}^{n}\frac{l'_n}{2n+1}T^{\sigma}_{nm}(t)\frac{\partial\bar{Y}_{nm}(\lambda,\theta)}{\partial\lambda} \\
\delta n(\lambda,\theta,t) &= l'_1 \vec{\mathbf{G}}_{CE-CM}\cdot\vec{\mathbf{e}}_{\mathbf{n}} + \delta\vec{\tau}\cdot\vec{\mathbf{e}}_{\mathbf{n}} - \delta\vec{\epsilon}\cdot\vec{\mathbf{e}}_{\mathbf{e}} \\
&+ \frac{3a\rho_w}{\rho_e}\sum_{n=2}^{N}\sum_{m=-n}^{n}\frac{l'_n}{2n+1}T^{\sigma}_{nm}(t)\frac{d\bar{Y}_{nm}(\lambda,\theta)}{d\theta} \quad (6)
\end{aligned}
$$

Here the unit vectors in up, north and east direction are denoted respectively by, $\vec{\mathbf{e}}_{\mathbf{h}}, \vec{\mathbf{e}}_{\mathbf{e}}, \vec{\mathbf{e}}_{\mathbf{n}}$. The degree 1 load Love numbers are frame dependent and must be given in the center of figure (CF) frame, when working with GPS *Blewitt and Clarke* [2003]. We use here the values derived from the Gutenberg-Bullen model, $h'_1 = -0.269$ and $l'_1 = 0.134$ *Farrell* [1972]; *Blewitt and Clarke* [2003]. Equation 6 shows that a degree 1 deformation and a pure translation and rotation (to absorb possible residual network shifts and rotations) can be estimated simultaneously as the degree 1 load Love numbers are substantially different from 1.

Munekane [2007] observed that residual variations of the network scale, expected from unmodelled second-order ionospheric delay in GPS analysis, are significantly smaller as compared to scale variations estimated jointly with geocenter motion from a global GPS loading inversion.

However, the station coverage and distribution of the global GPS networks is far from being sufficient for loading inversion from using only this data source. Whereas number and distribution of stations would allow only low-degree mass anomaly solutions from the data, the displacement of an individual station cannot be modelled sufficiently through such low-degree expansions. Furthermore, it is not clear to what extent systematic GPS technique errors map into load mass solutions.

2.1.3. Ocean Bottom Pressure changes

The bottom pressure, P, expressed in equivalent water height, at a certain point can be obtained from integrating the masses in the overlying oceanic and atmospheric mass column.

$$P(\lambda,\theta,t) = \int_{-H}^{0}\frac{\rho(\lambda,\theta,t,z)}{\rho_w}dz + \eta(\lambda,\theta,t) + \frac{p_0(\lambda,\theta,t)}{g\rho_w} \quad (7)$$

(adapted from *Böning et al.* [2008]) where H is ocean depth, η the sea surface elevation, ρ the depth dependent density, g the acceleration of gravity, and p_0 the atmospheric sea-level pressure. The atmospheric surface pressure and the surface elevation strongly interact, which can roughly be approximated by an IB response. When retrieving bottom pressure from ocean models it is therefore desirable to have a model which is also forced by atmospheric pressure and has a consistent surface response. For our purpose we assume that the 'zero' level coincides with the instantaneous geoid.

After subtracting an appropriate time mean we can relate the ocean bottom pressure change at a certain point to the solution vector:

$$
\begin{aligned}
\delta P(\lambda,\theta,t) &= \Delta M_0 + \frac{\rho_e}{\sqrt{3}\rho_w}\vec{\mathbf{e}}_{\mathbf{h}}(\lambda,\theta)\cdot\vec{\mathbf{G}}_{CE-CM} \\
&+ a\sum_{n=2}^{N}\sum_{m=-n}^{n}T^{\sigma}_{nm}(t)\bar{Y}_{nm}(\lambda,\theta) \quad (8)
\end{aligned}
$$

The unknown mass correction, ΔM_0, is constant for all points considered and absorbs the mass deficiency in the ocean model.

3. Data

The data for this study is three-fold: (1) We process GRACE L1b instrument data to weekly quasi-static, spherical harmonic models of gravity. These are then referred to the mean field in the period 2003-2007, and converted to harmonic coefficients of surface loading together with their full covariance matrix. Short-term atmospheric and oceanic mass variations are removed prior to gravity processing, and the weekly average of these models is restored to the weekly models. (2) We convert IGS station coordinates from weekly SINEX files to time series of displacements, referring to the mean of the period 2003-2007, and their full covariance. These are then related to weekly spherical harmonic models of surface loading mass using methods outlined in *Kusche and Schrama* [2005]. (3) We obtain grids of ocean bottom pressure from the Finite Element Sea-ice Ocean Model (FESOM, *Timmermann et al.* [2009]). These are converted to equivalent water heights, binned into weekly averages, referred to the mean in 2003-2007. Using the observation equations from the previous sections we construct for each dataset a normal equation, containing surface loading coefficient up to degree 30, a geocenter motion and data specific nuisance parameters. We then minimize the cost function of eq. 3, by combining and solving the normal equations on a weekly basis.

As this study is concerned with short term behaviour, no correction for glacial isostatic adjustment is made, any remaining trends should therefore be treated with caution. The study of trends, in particular for GPS, is a complicated issue which we hope to address in future research.

3.1. GRACE

Operational state of the art GRACE gravity field solutions are calculated by the GRACE Science Data System, established in a joint effort between GFZ, CSR and JPL, on a monthly basis up to degree and order 120. The latest release 04 (RL04) series of GFZ is called EIGEN-GRACE05S

(*Schmidt et al.* [2007a]). However, relevant mass variations such as barotropic Rossby waves, continental water storage changes, Earth's geocenter motion or solid Earth and ocean tides all take place at ten-daily or even shorter time scales. To address this problem, GFZ Potsdam generates GRACE gravity field products with increased temporal and decreased spatial resolution (*Dahle et al.* [2008]). These products are also based on EIGEN-GRACE05S standards and are currently available at the ISDC site (http://isdc.gfz-potsdam.de) for validation purposes as well as for science applications.

Consequently, we use these products in our joint GPS, OBP and GRACE inversion to provide more robust low to medium degree gravity field harmonics. To be consistent, the GRACE temporal resolution has been aligned to the GPS calendar week.

To investigate the resulting decrease in spatial resolution and to figure out the maximum spherical harmonic degree and order (N_{max}) for weekly GRACE solutions, a ground track analysis based on predicted orbits for the GRACE-A satellite has been performed. Here, in a first step the ephemeris data of the predicted orbits, which are given in 60 second intervals in the Conventional Terrestrial System (CTS), have been interpolated by a cubic polynomial interpolation to intervals of 5 seconds (the nominal step size of GRACE orbit integration) and then transformed to ellipsoidal coordinates (λ, θ, h) and stored in weekly ASCII tables. To take into account the actual GRACE data availability, a second table for each GPS week has been generated containing only those epochs corresponding to the real processed GFZ RL04 arcs. In a next step, two values per GPS week for the maximum distance of neighbouring ground tracks ($\Delta\lambda_{max}$) have been derived from both tables at a reference latitude of $\varphi_{ref} = 35°$, where, in general, the largest track separation occurs. The N_{max} values were then derived by the simple formula $N_{max} = 180°/\Delta\lambda_{max}$.

The results of the ground track analysis are shown in figure 1. It becomes obvious that the spatial resolution for the GRACE weekly solutions is limited by two factors: orbit configuration and data availability. As the ground track coverage varies in time due to changing orbit configuration of the GRACE satellites during mission lifetime, the N_{max} also vary in the range from about 30 to 50. The worst case has occurred in September 2004 (around GPS week 1290) where GRACE experienced a 4d repeat cycle. Besides this effect, the spatial resolution is further limited by data gaps as the N_{max} are in general clearly correlated ($\rho = 0.74$) with the number of processed days per week (cf. figure 2). However, for some weeks we got a small result for N_{max} although there is a satisfying amount of data available. For the period from August 2002 till February 2008, i.e. almost the entire time span of the GRACE mission, we got for 86 % of the GPS weeks an $N_{max} \geq 20$ and still 66 % of the GPS weeks have an $N_{max} \geq 30$.

Based on the results of the ground track analysis, it has been concluded that the best agreement between spatial resolution and quality of the standard GRACE weekly solutions will likely be achieved if N_{max} is set to 30, and we have adopted this resolution for our joint inversion procedure as well. The resulting GRACE GFZ RL04 'pure weekly solutions' for GPS Weeks 1177 to 1467 (August 2002 till February 2008) are each based on one 7-day batch of daily GRACE normal equation systems and no further constraints have been applied (in this study, GPS weeks 1200 up to 1408 have been used). All processing standards and background models are identical to the GRACE GFZ RL04 monthly gravity field models. Altogether, only 7 weeks are missing (4 weeks in June 2003 and 3 weeks in January 2004, where also the two standard monthly solutions are not available due to missing instrument data).

We would like to mention that, as an alternative method, a moving average approach has been implemented for GRACE only. This so-called 'pseudo-weekly solutions' each consist of five 7-day batches of GRACE normal equation systems. The two weeks before and after the central week are down-weighted according to the weighting scheme [0.25/0.5/1.0/0.5/0.25]. For the solution of the following week, the whole system is shifted by one week. As more data is used in this approach, the N_{max} could be increased to 60.

Time series of both weekly solutions have been compared to the corresponding results of the GFZ RL04 monthly GRACE models. Although the pure weekly solutions show a larger variability, they generally agree well with the monthly solutions. For some weeks, larger deviations are visible which do not necessarily correlate with the results of the ground track analysis. Therefore, it seems to be plausible that some of these 'outliers' rather represent physically induced signal than noise. For validation of the GRACE weekly solutions in the spatial domain, the RMS variability of surface mass anomalies (mainly representing continental hydrology) has been investigated as well. The comparison of 50 pseudo-weekly models in the year 2006 with the corresponding 12 GRACE GFZ RL04 monthly models, both filtered with a Gaussian filter of 500 km, indicates that the spatial distribution as well as the signal amplitude of the pseudo-weekly solutions is almost identical to those of the monthly solutions.

The formal error-covariance of GRACE is too optimistic and in joint inversion schemes this might cause an unrealistic 'over-weighting' of GRACE data. For example, it is known that the C_{20} coefficient is effected by tidal aliasing. We therefore calculated a degree dependent calibration scale for the solutions according to *Schmidt et al.* [2007b]. First, the annual signals and trends are removed from the weekly solutions. Then, the residual degree variances, including possible interannual signal, are considered to be remaining errors in the solutions. Using almost all weekly solutions, some weeks with anomalous bad coverage were excluded, we construct a best fitting degree dependent scale factor between the formal error and the 'mean error' constructed. Before the inversion, we rescale the error-covariance of the weekly solutions by these scale factors.

Unfiltered GRACE solutions display strong non-physical stripes in North-South direction, which are generally accepted to be caused by the directional weakness of the GRACE measurement geometry in combination with temporal aliasing. This phenomena mainly manifests itself as a correlation between coefficients sharing the same order and degree parity (*Swenson and Wahr* [2006]). In the formal error covariance matrix this is also visible as a dominant block diagonal structure with a chess board pattern (*Kusche et al.* [2009]). It is thought that subweekly aliasing signal (e.g. tide model errors) will propagate as non-Gaussian noise into the weakest part of the solution, casuing the striping pattern. We therefore use the full covariance information from GRACE to allow GPS and OBP to partly compensate the weakness in the GRACE measurement geometry.

In order to prepare the GRACE solutions for the inversion, we restore the weekly average of the high frequency ocean and atmospheric variations (GAC product) which were subtracted during the gravity field determination process. The weekly normal systems, which are expressed in potential coefficients, are then converted to surface loading normal systems by applying equation 5.

Consider the normal equation expressed in potential coefficients, $\hat{\mathbf{x}}^\phi$, its right hand side vector $\mathbf{b}^\phi$ and the normal matrix, $\mathbf{N}_\phi$:

$$\mathbf{N}_\phi \hat{\mathbf{x}}^\phi = \mathbf{b}^\phi \tag{9}$$

We can construct the new normal equation expressed in surface loading coefficients from the normal equation of eq. 9.

$$\begin{aligned} &\mathbf{N}_\sigma \hat{\mathbf{x}}^\sigma &&= \mathbf{b}^\sigma \\ \text{with} \quad &\mathbf{N}_\sigma &&= \mathbf{D}_\sigma \mathbf{D}_{\mathbf{cal}}^{-1} \mathbf{N}_\phi \mathbf{D}_{\mathbf{cal}}^{-1} \mathbf{D}_\sigma \\ \text{and} \quad &\mathbf{b}^\sigma &&= \mathbf{D}_\sigma \mathbf{D}_{\mathbf{cal}}^{-1} \mathbf{N}_\phi \mathbf{D}_{\mathbf{cal}}^{-1} (\mathbf{N}_\phi^{-1} \mathbf{b}^\phi) \end{aligned}$$

Here the diagonal calibration matrix, $\mathbf{D}_{\mathbf{cal}}$, contains the degree dependent scale factors. $\mathbf{D}_\sigma$ is a diagonal conversion matrix with elements derived from eq. 5 which relates the surface loading part of the unknowns vector, $\hat{\mathbf{x}}^\sigma$, to the solved vector of the potential coefficients of degree 2 and higher. The original normal matrix, $\mathbf{N}_\phi$, does not need to be inverted in the calculation of $\mathbf{N}_\sigma$.

3.2. GPS

In this work, we use published weekly combination solutions from the International GNSS Service (IGS). Station coordinates and the corresponding variance-covariance matrix are extracted from the SINEX files and aligned to ITRF05 using published transformation parameters. They are then transformed into residual displacements in the local North-East-Up frame referring to the mean station position and velocity in the time frame 2003-2007.

Time series are cleaned in two steps (*Kusche and Schrama* [2005]): First, we remove stations with obvious discontinuities in time and those which have short (smaller than 1 year) continuous observation periods. Second, we perform a GPS-only loading inversion up to degree 7. We exclude those stations which show large residuals wrt. the GPS-only fit, based on a 3σ rule. These are stations which are either very noisy, stand out compared to neighbouring stations, or are dominated by signal which do not fit the Love-Shida hypothesis we assume in the model (e.g. stations, effected by co/post-seismic phenomena, which display a strong toroidal component). The number of retained IGS stations for the subsequent analysis is then above 200 for most of the time (see figure 1), after about 1 % of the data is removed in the data snooping.

For this work, reprocessed IGS station coordinate solutions (*Rülke et al.* [2008]) have not yet been available. These will be used in follow-on investigations.

3.3. Ocean model

To simulate ocean mean state and variability the Finite Element Ocean Model (*Danilov et al.* [2004, 2005]), which uses the hydrostatic primitive equations, has been coupled to a finite element dynamic-thermodynamic sea-ice model. The dynamic part of the sea-ice model uses an elastic-viscous-plastic rheology. It includes a prognostic snow layer, but ignores internal heat storage. The resulting Finite Element Sea-ice Ocean Model (FESOM, *Timmermann et al.* [2009]) is initialised with temperature and salinity from the January mean dataset of the World Ocean Atlas (WOA01) and runs in time steps of 2h from 1958 to 2007. Atmospheric forcing consists of 10-m wind, 2-m temperature, specific humidity, total cloudiness, and net precipitation derived from the NCEP/NCAR reanalysis products, where net precipitation is derived from total precipitation and latent heat flux. To close the freshwater cycle, river runoff from the HDM model (*Walter* [2008]) is introduced into FESOM as a local volume flux. River runoff is scaled in order to ensure that the global mean freshwater budget is in equilibrium on time scales of 5 years and longer (*Böning et al.* [2008]). To achieve an appropriate description of bottom pressure variablity we apply the correction of *Greatbatch* [1994].

The model fields are discretized on a tetrahedral grid whereas the nodes of the 26 z-levels are aligned under the surface nodes. The mean horizontal grid spacing is 1.5°. To ensure a realistic representation of bathymetry, the bottom nodes are allowed to deviate from the z-levels. To minimize pressure gradients here, we consider only density anomalies and subtract a constant reference pressure as a function of depth. The model has been carefully validated and features a largely realistic ocean circulation and sea-ice distribution (*Timmermann et al.* [2009])

We obtain ocean bottom pressure from the FESOM simulations by applying eq. 7 with the model output and atmospheric forcing. Pressure anomalies are then formed by substracting a mean pressure.

$$\delta P(\lambda, \theta, t) = \frac{p(\lambda, \theta, t) - \bar{p}(\lambda, \theta)}{g\rho_w} \tag{10}$$

These are temporally (following the GPS week-count) and spatially (in $5^\circ \times 5^\circ$ cells) averaged, and collected in the vector $\mathbf{y}_{\mathrm{OBP-MOD}}$ (cf. eq. (3)).

It is very difficult to assess the actual level of errors in the modelled OBP values. We plan to investigate these errors in the near future by model simulations with different numerical parameterization and forcings, by comparisons with data from bottom pressure recorders, and from the inversions scheme itself that is described here. At the moment however, we simply assume that our modelled OBP suffers from an unknown overall offset, and that, at the equator, each $5^\circ \times 5^\circ$ cell may be corrupted by an uncorrelated error of $\sigma_{\mathrm{OBP}} = 3\,\mathrm{cm}$ level. To account for the area decrease at higher latitudes we additionally divide each cell error by $\sin\theta$.

Wu et al. [2006] assume an uncertainty of $\sigma = 1.7\,\mathrm{cm}$ for monthly averages in $1^\circ \times 1^\circ$ cells, on the basis of Topex/Poseidon errors. This would imply for weekly $5^\circ \times 5^\circ$ averages $\sigma = 1.7 \times \sqrt{4/25} = 0.7\,\mathrm{cm}$. The scheme we employ here is therefore more conservative. This has several reasons. The ocean model we use here does not assimilate altimetry data and can therefore be expected to be more inconsistent with real observations. Furthermore, the amount of grid points is large compared to for example the amount of GPS stations. Depending on the accuracy assumed, adding the model data in the inversion therefore acts as a strong regularization on the total solution *Jansen et al.* [2009]. Although we trust the dynamic topography and high resolution features of the model output, possible low degree inconsistencies, due to the lack of gravitational geoid changes caused by land sources and good river-runoff forcing in the model, have the potential to dominate the accurate lower degree information from GRACE. For the OBP accuracy used we found a good trade-off between the contribution of GRACE and OBP in the low to mid degree range (see fig. 3). The problems pointed out above should be seen as a strong motivation to construct more appropriate error models for ocean models.

4. Results

4.1. Data weighting

In a multi-sensor analysis problem, weighting of the different data sets plays a crucial role. Note that $\kappa = \beta = \gamma$ in eq. 3 would mean that all data sets be weighted relative to each other according to their formal uncertainties, as detailed in the previous chapter. However, we found that in this case the solution is largely dominated by the OBP model values and that we had to relax γ, by assuming a larger uncertainty, to allow GPACE and GPS to contribute to low- and mid-degree coefficients (*Jansen et al.* [2009] for a thorough discussion). Also, it is known that the formal GRACE errors underestimate the level of errors, in particular at low degrees, and that the formal GPS errors do not take into account several uncertainties of the GPS analysis.

We experimented with several choices of the parameters κ, β, γ in $\mathcal{L}_{\kappa,\beta,\gamma}$ as well as the GRACE error covariance. Here, we consider 4 different combination schemes. The first is a GPS-OBP-GRACE combination with the formal errors as described in the paper. The second scheme assumes an increased error, $\sigma = 4.8\,\mathrm{cm}$ for the FESOM data only. In order to study the effect of GRACE on the inversion we also constructed an inversion with only GPS and OBP, i.e. setting β to zero and using the described formal errors for FESOM and GPS. Finally, by masking out pixels of the ocean model at high latitudes ($|lat| > 72.5°$), we created a set which may mimic the latitude restriction we see in other models.

For a degree 30 inversion, the GPS+OBP combination is relatively unstable over land because of the lack of a dense enough GPS network. In order to maintain the spatial resolution over the ocean, we chose to apply a constraint assuming a signal variance of $(4\,\mathrm{cm})^2$ for the mean land variability. From weekly averages from the Watergap Global Hydrological Model (WGHM) (*Döll et al.* [2003]), we found a realistic mean land variation of $(2\,\mathrm{cm})^2$. Our choice thus allows for a larger variation and is a weaker constraint. This method is the same as the regularization method of *Kusche and Schrama* [2005] except that it is applied over land. We do not constrain the geocenter motion parameters.

Figure 3 shows the signal/error degree power spectra of the various weighting schemes and GRACE only, and of a (modelled) global geophysical dataset constructed from the GAC product and WGHM. The curves represent the mean variation over the period 2003-2007.

Its is clear from fig. 3 that the GRACE-only solutions (black curves) contain too much power in the high degree part of the spectrum. Its formal error is too optimistic, but the calibration procedure scales this to more realistic values. The GPS-OBP-GRACE combinations contain less power in the high degree spectrum but are still influenced by GRACE errors. The relative influence of GRACE increases mainly in the high degree part of the spectrum when we assume a larger error for FESOM.

From fig. 3 the OBP+GPS combination appears stable for low degrees. The effect of the regularization is clearly visible for degrees of 15 and larger, where the curve start to bend downward. Spatially however, the effect of regularization would only be visible over the continental surfaces.

The potential of the joint inversion is clear from inspecting the formal errors. Using the combinations we find strong improvements over GRACE only and GPS-OBP, where it must be remarked that they depend on the assumed accuracies.

The combination with the latitude restricted FESOM values shows little difference with the red curve in fig. 3 and is therefore not plotted. The explanation is that the latitude weighting of the FESOM data causes GRACE to mainly determine the solution in the polar regions.

Future work should focus on calibrating the weighting scheme from the data fits, while accounting for formal contribution measures and redundancy decomposition.

4.2. Parameter Correlation

It is important to study how well important parameters can be separated from the available datasets. Therefore we extracted a correlation matrix from the formal error-covariances of the inversion for two combination scenarios (using the full set and the GPS-OBP set). The results are plotted in figure 4.

Striking is, in the GPS-OBP-GRACE combination, that the separation of the residual Helmert parameters from the load moment vector (expressed in geocenter motion) causes no big problems in the inversion. In other words, the estimation of a rigid network translation/rotation together with a degree 1 deformation poses no problems in joint inversion schemes like those considered here. Significant correlations exist between the residual Helmert parameters themselves but this is unimportant as long as we consider the transformation as a whole as a nuisance. The residual Helmert parameters are however negatively correlated with the mass correction parameter, suggesting to handle this parameter with some care.

For the GPS-OBP combination, parameter correlations are increased. In particular we see increased correlations between the geocenter, and degree 2 coefficients and we see some correlations being introduced between the residual Helmert parameters and the geocenter motion.

Considering the above we conclude that GRACE contributes to the separation of the geocenter motion from the other unknowns, although it cannot directly sense it. As we will see later in section 4.5, the estimated geocenter motion is significantly changed by the addition of GRACE.

4.3. Comparison with in situ bottom pressure recorders

In order to validate our results, we have compared the combination solutions with time series of local ocean bottom pressure variations measured in the southern Indian ocean. The observations are the same series as used by *Rietbroek et al.* [2006]. They are detided with a harmonic analysis method and are averaged over and aligned to GPS weeks. The recorders were installed in the southern Indian Ocean at a depth of 4 km at the beginning of 2004 and were recovered a year later.

Figure 5 shows the timeseries of the bottom pressure recorders (BPRs) and our solution at the corresponding locations. To reduce any residual stripes in the solution, we applied a decorrelation filter (DDK2) as described in *Kusche et al.* [2009]. Furthermore, for comparison purposes, we also plotted the time series of the monthly and weekly decorrelated GFZ RL04 solution and the linearly interpolated values from FESOM.

In contrast to the global solutions, the local measurements are point measurements. To increase the spatial coherence between the local and global datasets we also constructed a mean series by averaging the data from the two

BPRs. These time series are also plotted in figure 5.

Similar to the results of *Rietbroek et al.* [2006] our solutions have strong correlations,0.7-0.8, with the local measurement series (see tab. 1). The RMS of the difference of the series vary between 2.2 cm for Crozet to 1.8 [cm] for the mean at the midpoint.

FESOM derived series are also capable of capturing the high frequency variations. Compared to the combination results, for the Kerguelen station we find a stronger correlation (of 0.8), for the FESOM series. Compared to the combination and in situ series we find that FESOM slighty underestimates the variability. Inspecting figure 5, we see that this can be attributed to the weaker annual component. For the midpoint we find an annual amplitude of 6 mm for FESOM while the BPR and the combination solution yield amplitudes of 33 mm and 13 mm respectively.

Due to the shorter averaging window, we find stronger high frequency variations than *Rietbroek et al.* [2006]. Figure 5 shows that quite a few high resolution features are captured both by the combination solution and the FESOM output. In fact, many of those features dissapear when we consider monthly averages of GRACE only, as shown by the red curve in figure 5.

Using GRACE only solutions at weekly time resolution we find weaker correlations in the order of 0.4-0.5. From table 1 it is clear that the combination solution provides a strong improvement over the weekly solutions both in correlation and in residual RMS.

4.4. Mean ocean bottom pressure and mass change

By application of eq. 2 to the inverse GRACE/GPS/OBP solutions, time series of total (ocean-averaged) variations in ocean bottom pressure $\Delta M(t)$ are obtained. On the other hand, the total variation may be obtained integrating the FESOM grid anomalies over the ocean surface and optionally correcting for the estimated mass correction term, ΔM_0:

$$\Delta M(t) = \int_{\Omega} O(\lambda,\theta)\delta P(\lambda,\theta,t)\sin\theta d\theta d\lambda - \Delta M_0(t) \quad (11)$$

Expressing total OBP variations through eq. 2 or 11 would be equivalent considering a spherical harmonic and a gridded data set respectively, as the surface loading and the correction term for the gridded pressure values are estimated jointly. However in eq. 2 spherical harmonic truncation and possibly spectral smoothing are involved, which, together with the coastline resolution, leads to small differences (about 1.6 mm RMS) in the two time series.

In order to retrieve the variation of the ocean mass we have to subtract the atmospheric component from the total ocean bottom pressure. In this study, we use the weekly averaged ECMWF pressure fields expressed in spherical coefficients (weekly GAA product). Because of the lack of good atmospheric error models we are forced to postulate that the errors are much smaller than the signal observed here. As the atmospheric models are assimilating pressure data we assume that the output is close enough to reality.

Figure 6 shows the time variation of the total ocean bottom pressure for the uncorrected FESOM model data and the combination solution. Furthermore, the power spectral density of the series, where we removed an annual and semi-annual harmonic, is also shown. In the same figure on the right, we split up the total ocean bottom pressure in an atmospheric component from the weekly GAA product and the remaining oceanic component. Annual amplitudes and phases from the harmonic fit are plotted in figure 7. Since FESOM is forced with NCEP we correct it with the NCEP ocean mean to retrieve a field more consistent with the initial model.

Observing figure 7, we find that the uncorrected FESOM model displays the strongest annual variation in ocean bottom pressure (annual amplitude 11.2 mm, annual phase 246.9d, semiannual amplitude 0.9 mm, semiannual phase 67.4d). When we subtract the atmospheric part, i.e. the NCEP product, we find a smaller variation with a strong phase shift (annual amplitude 9.0 mm, annual phase 286.6d, semiannual amplitude 0.7 mm, semniannual phase 8.2d).

The results from our combination solution indicate smaller annual amplitudes (8.7/7.4 mm OBP/ocean mass) accompanied by minor phase shifts (cf. table 2).

The removal of the high latitude information from FESOM decreases the annual amplitudes by approximately 0.6 mm. Using the latitude restricted ECCO model, *Wu et al.* [2006] obtained results matching to within 0.3 mm amplitude and 7 days phase. Our ocean mass solution shows a lower amplitude than that obtained by *Chambers et al.* [2004] independently from GRACE RL01 fields and from steric-corrected altimetry, but somewhat larger compared to *Willis et al.* [2008].

After removing an estimated annual and semiannual fit we find that the power spectra show strong subannual variation. Two main subannual spectral bands (3-4 cycle/year, 6-7 cycles/year) are visible in the ocean bottom pressure variations whereas the ocean mass variations exhibit a smoother power distribution (figure 6). The ocean mass variation of FESOM shows much smaller subannual variations, which is caused by the smoothness of the forcing fields of the model.

The OBP variations from the GRACE weekly solutions show an amplitude decrease of around 2.6 mm and a strong phase shift of about a month. This offset is almost entirely due to the geocenter motion, which is not considered in the GRACE-only estimates.

4.5. Geocenter motion

Figure 8 shows our weekly geocenter motion estimates together with an annual/semiannual fit. We compare three weighting schemes, the GPS-OBP-GRACE version, the combination with the zonally resticted FESOM and the GPS-OBP combination. Figure 9 shows the power spectral density of the geocenter motion without annual and semi-annual components (table 3).

We find virtually no change in the X and Y component and the estimated semi-annual curves for the two GRACE-OBP-GPS combinations. On the other hand the Z component changes somewhat in its annual component. The high latitude information from FESOM causes an increase of the annual amplitude from 1.9 mm to 2.5 mm. By inspecting fig. 8 and 9 we see however that the Z component is more noisier and seasonal fits may be easily distorted. On subannual timescales our zonally restricted combination is very similar to the one with full FESOM information. Although fig 9 shows a discrepancy at the highest frequencies.

Our GPS+OBP combination produces different results for the geocenter motion. In the X component we see a phase shift of about 30 days, while the amplitudes have comparable magnitudes. The largest differences occur for the Z component. We suspect that the discrepancies are due to the weaker separability of the unknowns as mentioned before.

Wu et al. [2006] also used a combination solution to retrieve geocenter motion. The annual and semi-annual amplitudes and phases are comparable to ours, with some exceptions. We find for example a stronger annual Y amplitude (4.5 wrt 2.5 mm) and there is an annual phase shift in the X component of about 30 days.

Compared to the more recent results of *Swenson et al.* [2008] we have larger annual amplitudes. We atrribute this feature mainly to the inclusion of GPS in our solution and the co-estimation of an ocean mass correction.

Table 3 shows an overall agreement between geocenter estimates in the range of a couple of months and several mm's in amplitude. The remaining discrepancies are in general above the reported standard deviations and could be caused by the different time ranges considered and technique specific errors *Feissel-Vernier et al.* [2006]. For example, they show that the estimated amplitudes vary strongly over the years and that different techniques and models produce different results.

Figure 9 shows that after the removal of the annual and semiannual fit a significant part of the spectral power goes into subannual frequencies. This is in particular true for the Z component and confirms the results of *Feissel-Vernier et al.* [2006].

4.6. Global mass correction ΔM_0 of FESOM

A spatially uniform mass correction for the FESOM model is estimated from our inversions. ΔM_0 is shown in figure 10, for three weighting schemes (red: Full FESOM coverage, blue: Full FESOM with increased error, green: FESOM $|lat| \leq 72.5°$) . Currently, we investigate how to optimally use the estimated mass correction to adjust the freshwater flux in future model runs.

For ΔM_0 from the combination solution, we find an RMS variability of 3 mm. The ΔM_0 estimate has a red spectrum, with power spread at frequencies between the annual and the semiannual periods, which is shown in figure 10.

For full FESOM coverage, the estimated standard deviation, $\sigma_{\Delta M_0}$, from the inversion is about 12 mm. When assuming slightly different errors for the FESOM data (4.8 cm per 5° x 5° grid) we found only small differences in the estimated mass correction (0.9 mm RMS). Therefore, we consider our estimated time-series as statistically significant.

4.7. Spatial maps of ocean bottom pressure change and ocean mass change

The addition of FESOM output in our inversion constrains the values of OBP over the ocean. We studied the differences between the original FESOM data and the inversion results. This residual is shown in Figure 11, which shows the annual components in terms of amplitude and phase (contours). At first sight, we see at higher spatial resolution the influence of the GRACE striations. There are however significant larger scale patterns visible. These patterns show that a significant part of the low resolution signal is determined by the addition of GRACE and GPS. In particular, we see a large area around south America, in the Arctic and in the Southern ocean were the BPRs were installed. The right hand side of figure 11 shows the difference of FESOM and the GPS+OBP combination. Although, there are virtually no GPS stations in the ocean, which might constrain the ocean model, we do see a weak but consistent degree 1 signal centered around south America. In the Arctic there is also a strong offset. For both scenarios, we believe that this Artic offset is geophysical signal which is added by the GRACE/GPS data sets. The FESOM output is known to be somewhat conservative in the Arctic while in situ pressure records in this region have shown strong variability (*Morison et al.* [2007]).

Spatial maps of the annual amplitude and phase of the estimated ocean mass change (OBP minus GAA) are provided in figure 12 (full combination and GPS+OBP). On the other hand we plotted the total RMS variability, with and without the seasonal terms, of the ocean mass changes in figure 13. We find that the major part of the ocean variability cannot be explained by annual varying signal but must be of subseasonal origin. In particular we find that at high latitudes significant variations occur.

In addition, we have investigated the temporal correlation of the ocean mass maps that we obtain from our inversion. To this end, for each grid point the autocorrelation

$$c(\lambda, \theta, n\Delta t) = \frac{\sum_{i=1}^{I-n} X(\lambda, \theta, t_i) X(\lambda, \theta, t_i - n\Delta t)}{\sum_{i=1}^{I} X(\lambda, \theta, t_i)^2} \quad (12)$$

has been computed for lags n of up to four weeks, after removing the dominating annual contribution from the ocean mass signals first. Maps of $c(\lambda, \theta, n\Delta t)$ are shown in figure 14 for ocean mass change. We see that for most parts of the ocean the mass change decorrelates quickly within 4 weeks. This suggests that most of the signal variations occurr at time scales shorter than a month. The strongest correlations appear at high latitudes, where we also expect a stronger oceanic signal. Although not shown here, we see a similar behavior for the OBP changes.

5. Conclusions

We have constructed a joint inversion solution of surface loading, in which we merged data from the IGS GPS network solution, GRACE and output from the coupled sea-ice model FESOM. Compared to GRACE only solutions, this combination approach allows the simultaneous estimation of the geocenter motion and a mass correction parameter for the ocean model together with a global spherical harmonic expansion of surface loading. At the same time we reduce the formal errors. We provide independent estimates of surface loading, up to spherical harmonic degree and order 30, every week.

The data weighting in the joint inversion, remains a difficult issue. We found that increasing the OBP error from 3 cm to 4.8 cm caused mainly a difference in the estimated higher degree coefficients, where GRACE errors became more dominant.

The use of latitude restricted ocean models has only a limited impact on the solutions, although this heavily depends on the assumed error model for the OBP set (in this study the latitude weighting diminishes its influence at higher latitudes). We do however see some indications that it can have an effect on the Z-component of the geocenter motion.

We have investigated the correlation, derived from the formal error-covariance matrix, between the estimated ocean model correction, the geocenter motion, residual Helmert parameters and degree 2 coefficients of surface loading. We found that the residual Helmert parameters, considered as nuisance, show little correlation with the geocenter motion. For the GPS+OBP combination correlations increase, showing a weaker potential of separating the parameters.

From the inversion we find an annual amplitude of the mean ocean bottom pressure variation of 8.7 mm peaking in August/September. After subtracting the weekly atmospheric pressure we obtain the variation of the ocean mass with an annual amplitude of 7.4 cm peaking in October. Removing the high latitude information from FESOM tends to decrease the amplitude by 0.5 mm and causes phase shifts of only 4 days. The results match those obtained by *Wu et al.* [2006], who also used a similar combination with ECCO data, closely.

The annual component of the estimated geocenter motion agrees reasonably with previous results, although we recognize that annual components vary strongly over time. The annual amplitudes of the X,Y and Z components are 2.1 mm, 4.5 mm and 2.5 mm respectively, whereas the series are peaking in March, December and March.

By comparing the GPS+OBP solution and the full combination solutions, we see that, although GRACE by itself can not solve for the geocenter motion, it does have a considerable influence on the estimated geocenter motion in joint inversion schemes.

The weekly resolution of our results allows the study of high frequency signals. We see that, over the ocean, the autocorrelation of the ocean mass quickly decreases when one increases the lag from 1 week to a month. At high latitudes we find the strongest autocorrelations (0.5), and variations ($\sigma = 10$ cm) of the ocean mass. This signal can be mainly attributed to subannual variations.

On a more regional scale, we compared the results with independent time series of in situ bottom pressure in the southern Indian Ocean. Comparing the local measurements with our results, we found strong correlations in the range of 0.7-0.8 and comparable variations. Furthermore, the joint inversion method tends to improve the annual component from the ocean model and at the same time reduce the noise from GRACE.

A significant part of the variation in the local series is due to submonthly features, which are also captured by the BPRs, the inversion solution and the FESOM model. These features must be of large spatial scales in order to be detected by our solutions.

Acknowledgments. The authors acknowledge support provided by the German Research Foundation (DFG) unders grants KU 1207/6-1, FL 592/1-1, SCHR779/4-1 within the Special Priority Program SPP 1257 Mass Transport and Mass Distribution in the System Earth. Furthermore, we would like to thank Pascal LeGrand who organized the financing and installation of the Indian Ocean BPRs with the help of IPEV (Institut Polaire Francais Paul Emile Victor) and POL (Proudman Oceanographic Laboratory). The helpful comments by two anonymous reviewers were greatly appreciated.

References

Blewitt, G., and P. Clarke (2003), Inversion of Earth's changing shape to weigh sea level in static equilibrium with surface mass redistribution, *Journal of Geophysical Research (Solid Earth)*, *108*, 2311–+, doi:10.1029/2002JB002290.

Böning, C., R. Timmermann, A. Macrander, and J. Schröter (2008), A pattern-filtering method for the determination of ocean bottom pressure anomalies from GRACE solutions, *Geophys. Res. Lett.*, *35*, doi:10.1029/2008GL034974.

Bouillé, F., A. Cazenave, J. , Lemoine, and J. Crétaux (2000), Geocentre motion from the DORIS space system and laser data to the Lageos satellites: comparison with surface loading data, *Geophysical Journal International*, *143*(1), 71–82, doi:10.1046/j.1365-246x.2000.00196.x.

Chambers, D., J. Wahr, and R. Nerem (2004), Preliminary observations of global ocean mass variations with GRACE, *Geophysical Research Letters*, *31*(13).

Chambers, D. P. (2006), Observing seasonal steric sea level variations with GRACE and satellite altimetry, *Journal of Geophysical Research (Oceans)*, *111*(C10), 3010–+, doi:10.1029/2005JC002914.

Chambers, D. P., M. E. Tamisiea, R. S. Nerem, and J. C. Ries (2007), Effects of ice melting on GRACE observations of ocean mass trends, *Geophysical Research Letters*, *34*, 5610–+, doi:10.1029/2006GL029171.

Chen, J. L., and C. R. Wilson (2008), Low degree gravity changes from GRACE, Earth rotation, geophysical models, and satellite laser ranging, *Journal of Geophysical Research (Solid Earth)*, *113*(B12), 6402–+, doi:10.1029/2007JB005397.

Chen, J. L., C. R. Wilson, and K.-W. Seo (2008), S2 tide aliasing in GRACE time-variable gravity solutions, *Journal of Geodesy*, pp. 66–+, doi:10.1007/s00190-008-0282-1.

Crétaux, J.-F., L. Soudarin, F. J. M. Davidson, M.-C. Gennero, M. Bergé-Nguyen, and A. Cazenave (2002), Seasonal and interannual geocenter motion from SLR and DORIS measurements: Comparison with surface loading data, *Journal of Geophysical Research (Solid Earth)*, *107*, doi:10.1029/2002JB001820.

Dahle, C., F. Flechtner, J. Kusche, and R. Rietbroek (2008), GFZ EIGEN-GRACE05S (RL04) Weekly Gravity Field Time Series, proceedings of the 2008 GRACE Science Team Meeting, San Francisco, http://www.csr.utexas.edu/grace/GSTM.

Danilov, S., G. Kivman, and J. Schroter (2004), A finite-element ocean model: principles and evaluation, *Ocean Modelling*, *6*, 125–150, doi:10.1016/S1463-5003(02)00063-X.

Danilov, S., G. Kivman, and J. Schröter (2005), Evaluation of an eddy-permitting finite-element ocean model in the North Atlantic, *Ocean Modelling*, *10*, 35–49, doi:10.1016/j.ocemod.2004.07.006.

Davis, J., P. Elósegui, J. Mitrovica, and M. Tamisiea (2004), Climate-driven deformation of the solid Earth from GRACE and GPS, *Geophys. Res. Lett*, *31*, 24.

Dobslaw, H., and M. Thomas (2007), Impact of river run-off on global ocean mass redistribution, *Geophysical Journal International*, *168*, 527–532, doi:10.1111/j.1365-246X.2006.03247.x.

Döll, P., F. Kaspar, and B. Lehner (2003), A global hydrological model for deriving water availability indicators: model tuning and validation, *Journal of Hydrology*, *270*(1-2), 105–134.

Farrell, W. E. (1972), Deformation of the Earth by Surface Loads, *Reviews of Geophysics and Space Physics*, *10*, 761–+.

Feissel-Vernier, M., K. Le Bail, P. Berio, D. Coulot, G. Ramillien, and J.-J. Valette (2006), Geocentre motion measured with DORIS and SLR, and predicted by geophysical models, *Journal of Geodesy*, *80*, 637–648, doi:10.1007/s00190-006-0079-z.

Greatbatch, R. J. (1994), A note on the representation of steric sea level in models that conserve volume rather than mass, *J. Geophys. Res.*, , *99*, 12,767–12,771, doi:10.1029/94JC00847.

Jansen, M., B. Gunter, and J. Kusche (2009), The impact of GRACE, GPS and OBP data on estimates of global mass redistribution, *Geophysical Journal International*, *177*(1), 1–13, doi:10.1111/j.1365-246X.2008.04031.x.

Kusche, J. (2007), Approximate decorrelation and non-isotropic smoothing of time-variable GRACE-type gravity field models, *Journal of Geodesy*, *81*, 733–749, doi:10.1007/s00190-007-0143-3.

Kusche, J., and E. J. O. Schrama (2005), Surface mass redistribution inversion from global GPS deformation and Gravity Recovery and Climate Experiment (GRACE) gravity data, *Journal of Geophysical Research (Solid Earth)*, *110*(B9), 9409–+, doi:10.1029/2004JB003556.

Kusche, J., R. Schmidt, S. Petrovic, and R. Rietbroek (2009), Decorrelated GRACE time-variable gravity solutions by GFZ, and their validation using a hydrological model, *Journal of Geodesy*, doi:10.1007/s00190-009-0308-3.

Moore, P., and J. Wang (2003), Geocentre variation from laser tracking of LAGEOS1/2 and loading data, *Advances in Space Research*, *31*, 1927–1933, doi:10.1016/S0273-1177(03)00170-4.

Morison, J., J. Wahr, R. Kwok, and C. Peralta-Ferriz (2007), Recent trends in Arctic Ocean mass distribution revealed by GRACE, *Geophysical Research Letters*, *34*, 7602–+, doi:10.1029/2006GL029016.

Munekane, H. (2007), Ocean mass variations from GRACE and tsunami gauges, *Journal of Geophysical Research (Solid Earth)*, *112*(B11), 7403–+, doi:10.1029/2006JB004618.

Ponte, R. M., K. J. Quinn, C. Wunsch, and P. Heimbach (2007), A comparison of model and GRACE estimates of the large-scale seasonal cycle in ocean bottom pressure, *Geophysical Research Letters*, *34*, 9603–+, doi:10.1029/2007GL029599.

Quinn, K. J., and R. M. Ponte (2008), Estimating weights for the use of time-dependent gravity recovery and climate experiment data in constraining ocean models, *Journal of Geophysical Research (Oceans)*, *113*(C12), 12,013–+, doi:10.1029/2008JC004903.

Rietbroek, R., P. LeGrand, B. Wouters, J.-M. Lemoine, G. Ramillien, and C. W. Hughes (2006), Comparison of in situ bottom pressure data with GRACE gravimetry in the Crozet-Kerguelen region, *Geophysical Research Letters*, *33*, doi:10.1029/2006GL027452.

Rülke, A., R. Dietrich, M. Fritsche, M. Rothacher, and P. Steigenberger (2008), Realization of the Terrestrial Reference System by a reprocessed global GPS network, *J. Geophys. Res.*, *113*(B08403), doi:10.1029/2007JB005231.

Salstein, D. A., R. M. Ponte, and K. Cady-Pereira (2008), Uncertainties in atmospheric surface pressure fields from global analyses, *J. Geophys. Res.*, *113*(D14107), doi:10.1029/2007JD009531.

Schmidt, R., U. Meyer, C. Dahle, F. Flechtner, and J. Küsche (2007a), Monthly and Weekly EIGEN-GRACE05S Gravity Field Solutions For Monitoring of Mass Variations in the Earth System, in *Second Space for Hydrology Workshop "Surface Water Storage and Runoff: Modelling, In-Situ data and Remote Sensing", Geneva (Switzerland)*, edited by J. Benveniste et al., ESA Publication WPP-280.

Schmidt, R., F. Flechtner, R. König, U. Meyer, K.-H. Nuemayer, C. Reigber, M. Rothacher, S. Petrovic, S.-Y. Zhu, and A. Günther (2007b), *Dynamic Planet*, chap. GRACE Time-Variable Gravity Accuracy Assessment, pp. 237–243, Springer Berlin Heidelberg, doi:10.1007/978-3-540-49350-1_36.

Stammer, D., C. Wunsch, and R. M. Ponte (2000), De-Aliasing of Global High Frequency Barotropic Motions in Altimeter Observations, *Geophysical Research Letters*, *27*, 1175–+, doi:10.1029/1999GL011263.

Swenson, S., and J. Wahr (2006), Post-processing removal of correlated errors in GRACE data, *Geophysical Research Letters*, *33*, doi:10.1029/2005GL025285.

Swenson, S., D. Chambers, and J. Wahr (2008), Estimating geocenter variations from a combination of GRACE and ocean model output, *J. Geophys. Res.*, *113*(B08410), doi:10.1029/2007JB005338.

Thompson, P. F., S. V. Bettadpur, and B. D. Tapley (2004), Impact of short period, non-tidal, temporal mass variability on GRACE gravity estimates, *Geophysical Research Letters*, *31*, 6619–+, doi:10.1029/2003GL019285.

Timmermann, R., S. Danilov, J. Schröter, C. Böning, D. Sidorenko, and K. Rollenhagen (2009), Ocean circulation and sea ice distribution in a finite element global sea ice-ocean model, *Ocean Modelling*, *27*(3-4), 114 – 129, doi:10.1016/j.ocemod.2008.10.009.

Wahr, J., M. Molenaar, and F. Bryan (1998), Time variability of the Earth's gravity field: Hydrological and oceanic effects and their possible detection using GRACE, *Journal of Geophysical Research*, *103*, 30,205–30,230, doi:10.1029/98JB02844.

Walter, C. (2008), Simulationen hydrologischer Massenvariationen und deren Einfluss auf die Erdrotation, Ph.D. thesis, Technical University Dresden, Dresden.

Wenzel, M., and J. Schröter (2007), The Global Ocean Mass Budget in 1993 2003 Estimated from Sea Level Change, *Journal of Physical Oceanography*, *37*, 203–+, doi:10.1175/JPO3007.1.

Willis, J., D. Chambers, and R. Nerem (2008), Assessing the globally averaged sea level budget on seasonal to interannual timescales, *Journal of Geophysical Research (Oceans)*, *113*(C12), 6015–+, doi:10.1029/2007JC004517.

Wu, X., M. B. Heflin, E. R. Ivins, and I. Fukumori (2006), Seasonal and interannual global surface mass variations from multisatellite geodetic data, *Journal of Geophysical Research (Solid Earth)*, *111*(B10), 9401–+, doi:10.1029/2005JB004100.

R. Rietbroek, Helmholtz-Centre Potsdam - GFZ German Research Centre for Geosciences, Telegrafenberg, D-14473 Potsdam, Germany, (roelof@gfz-potsdam.de)

S.-E. Brunnabend, Alfred Wegener Institute, Bussestrasse 24, 27570 Bremerhaven, Germany, (Sandra-Esther.Brunnabend@awi.de)

Ch. Dahle, Helmholtz-Centre Potsdam - GFZ German Research Centre for Geosciences, c/o DLR Oberpfaffenhofen, Münchener Straße 20, 82234 Weßling (dahle@gfz-potsdam.de)

F. Flechtner, Helmholtz-Centre Potsdam - GFZ German Research Centre for Geosciences, c/o DLR Oberpfaffenhofen, Münchener Straße 20, 82234 Weßling (flechtne@gfz-potsdam.de)

J. Kusche, Institute of Geodesy and Geoinformation, University of Bonn, D-53115 Bonn, Germany (kusche@geod.uni-bonn.de)

J. Schröter, Alfred Wegener Institute, Bussestrasse 24, 27570 Bremerhaven, Germany, (Jens.Schroeter@awi.de)

R. Timmermann, Alfred Wegener Institute, Bussestrasse 24, 27570 Bremerhaven, Germany, (Ralph.Timmermann@awi.de)

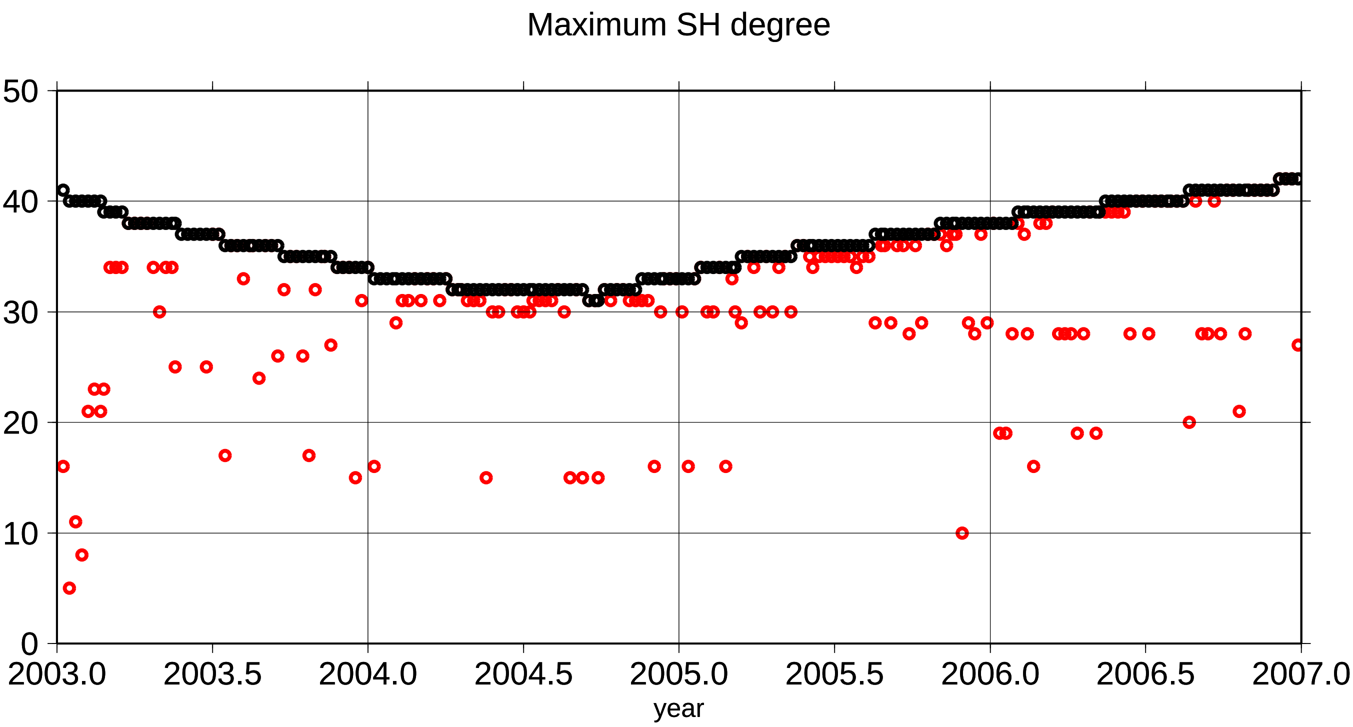

Figure 1. Maximum spherical harmonic degree N_{max} for GRACE weekly solutions depending on orbit configuration only (black circles) and depending on orbit configuration and data availability (red circles).

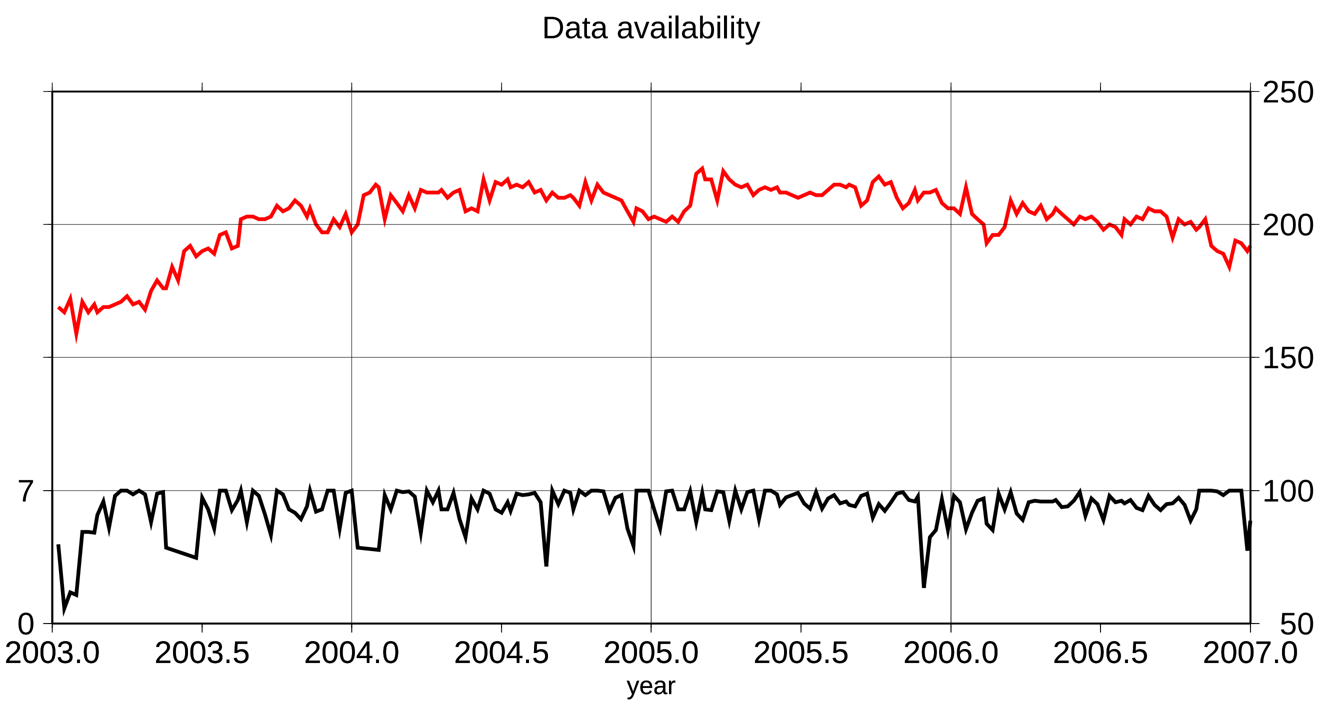

Figure 2. Data availability for GRACE weekly solutions (black line, in processed days per week) and for GPS (red line, used IGS stations per week).

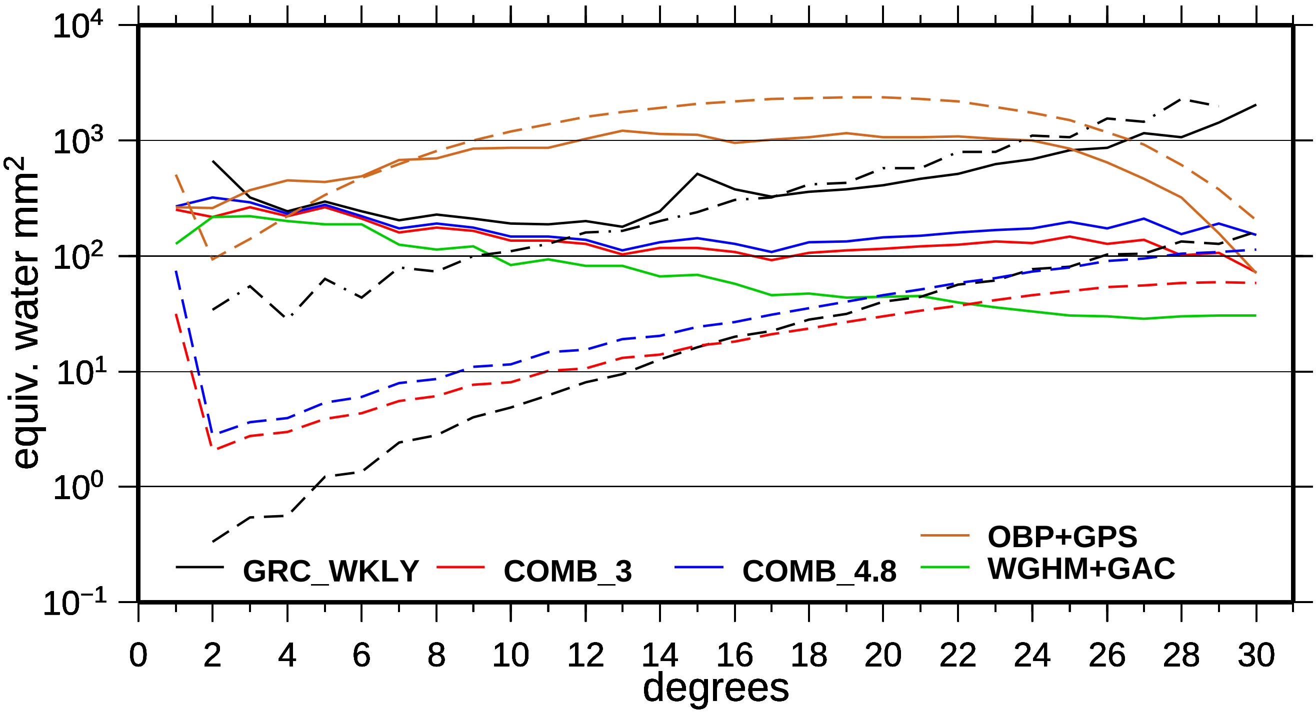

Figure 3. Mean signal (solid) and error (dashed) degree variances from the combination solutions (FESOM with σ of 3/4.8 cm), from a regularized OBP+GPS solution and weekly GRACE only (black). The dash-dot line represents the calibrated GRACE error.

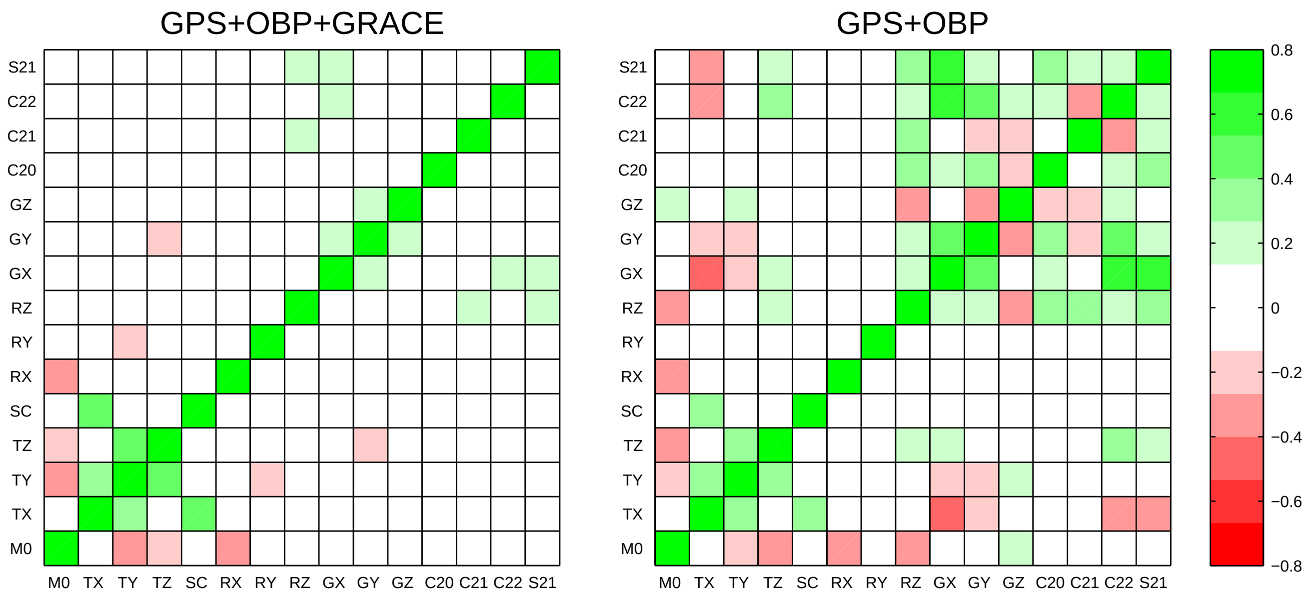

Figure 4. Subsection of the formal correlation matrix. Parameters included are ocean model mass correction, $M0$, residual Helmert parameters (translation $\delta\vec{\tau} \rightarrow$ T[X/Y/Z], rotation $\delta\vec{\epsilon} \rightarrow$ R[X/Y/Z], and scale $\delta s \rightarrow$ SC), the geocenter motion, G[X/Y/Z], and the degree 2 coefficients of surface loading, [S/C]2[0/1/2]. The flft matrix is derived from using the OBP, GRACE and GPS dataset, while the right matrix is derived from using only GPS and OBP.

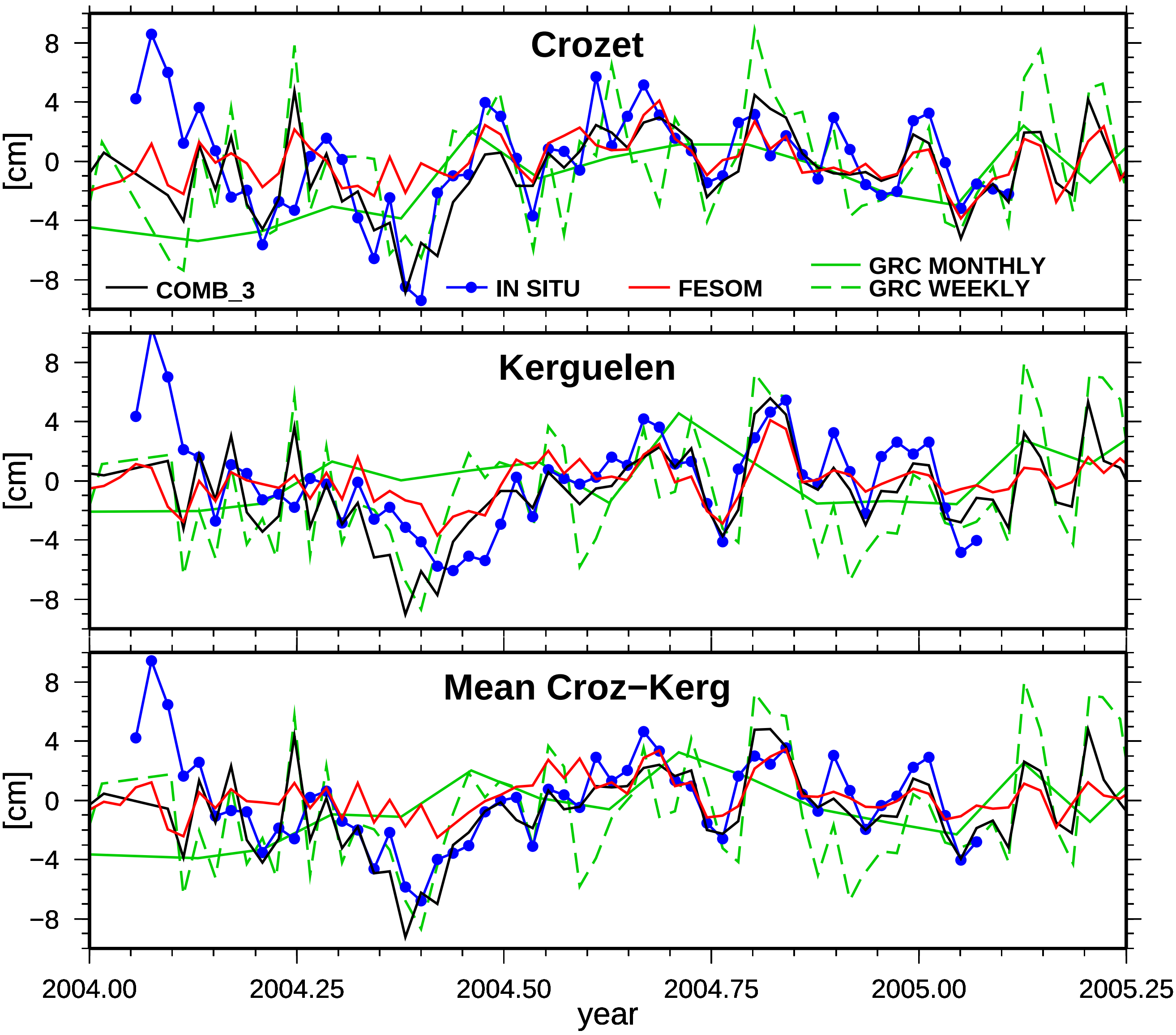

Figure 5. Time series of the in situ bottom pressure recorders (blue with circles) from *Rietbroek et al.* [2006], joint inversion (black solid), FESOM(red) and GRACE GFZ RL04 monthly and weekly solution (green solid and dashed respectively). Upper: Crozet $(54.9°E, 47.1°S)$. Mid: Kerguelen $(61.3°E, 48.8°S)$. Bottom: the midpoint between Crozet and the Kerguelen. The joint inversion and GRACE solutions are filtered with the decorrelation filter of *Kusche et al.* [2009].

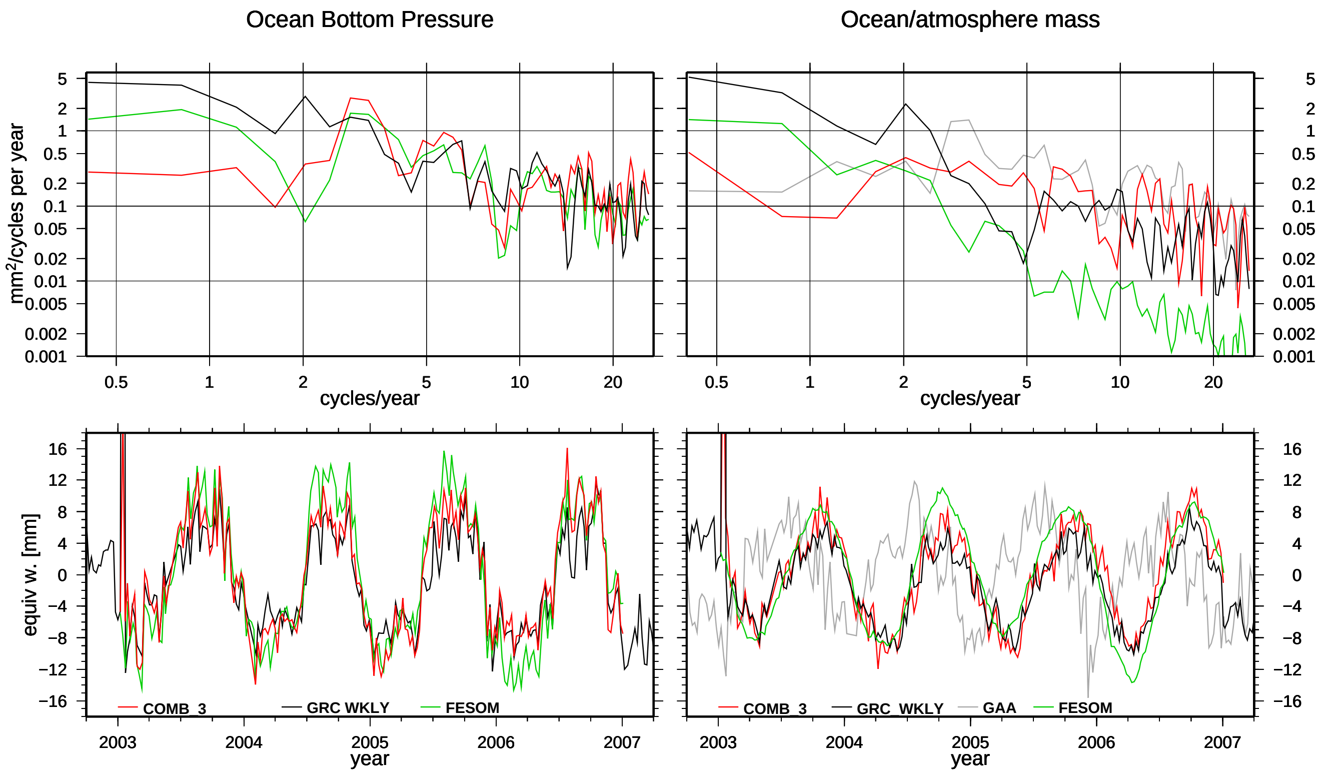

Figure 6. Time series and power spectra of ocean bottom pressure (left) and ocean/atmospheric mass variations (right). A seasonal fit was removed before calculating the power spectrum. red: combination solution, black: Weekly GRACE only solution, green: FESOM only data.

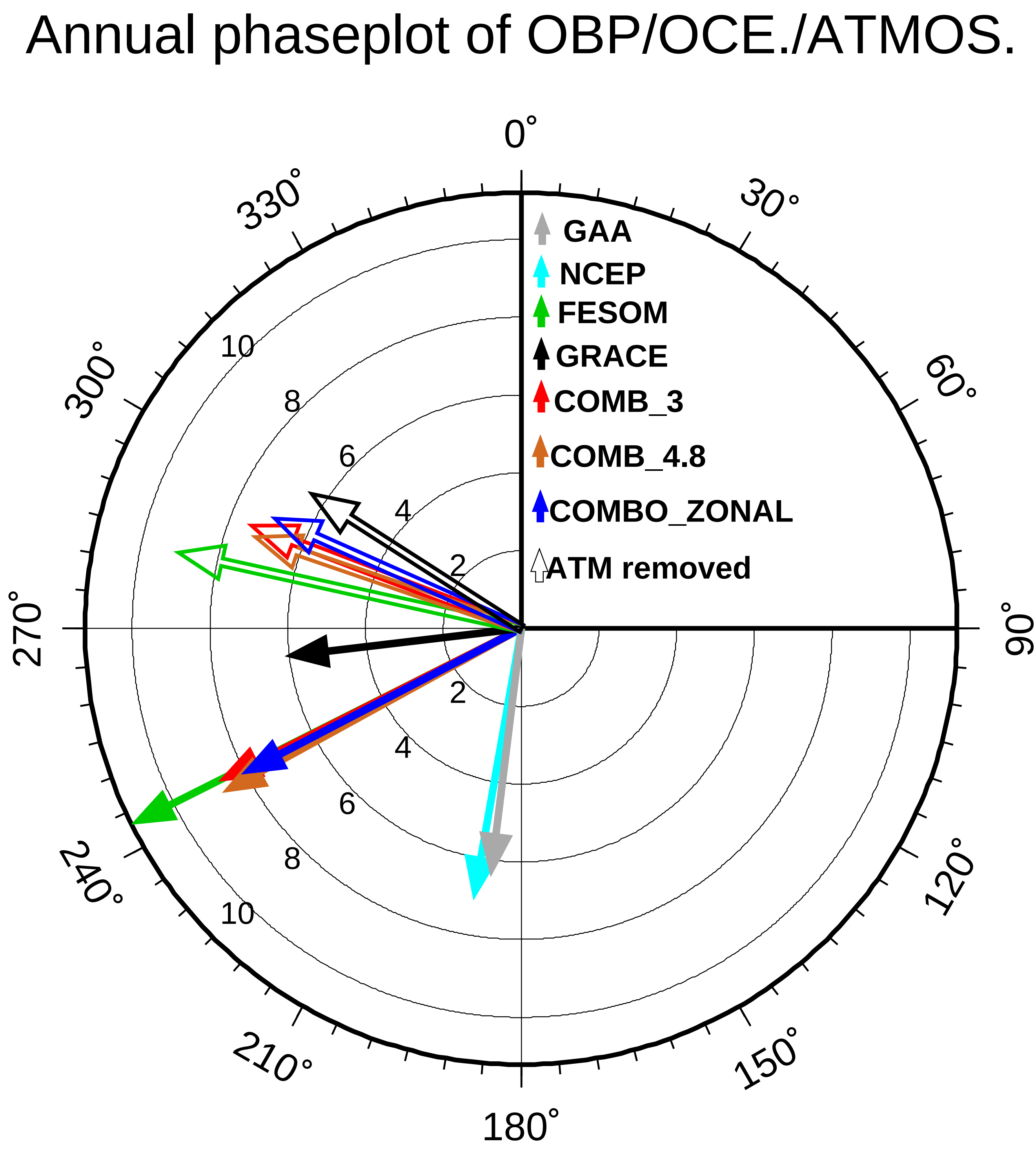

Figure 7. Phase plot of the fitted annual components of ocean bottom pressure and its separation into oceanic and atmospheric mass. Components are derived from an annual/semi-annual least squares fit to the time series. The GRACE only estimate does not contain any geocenter motion.

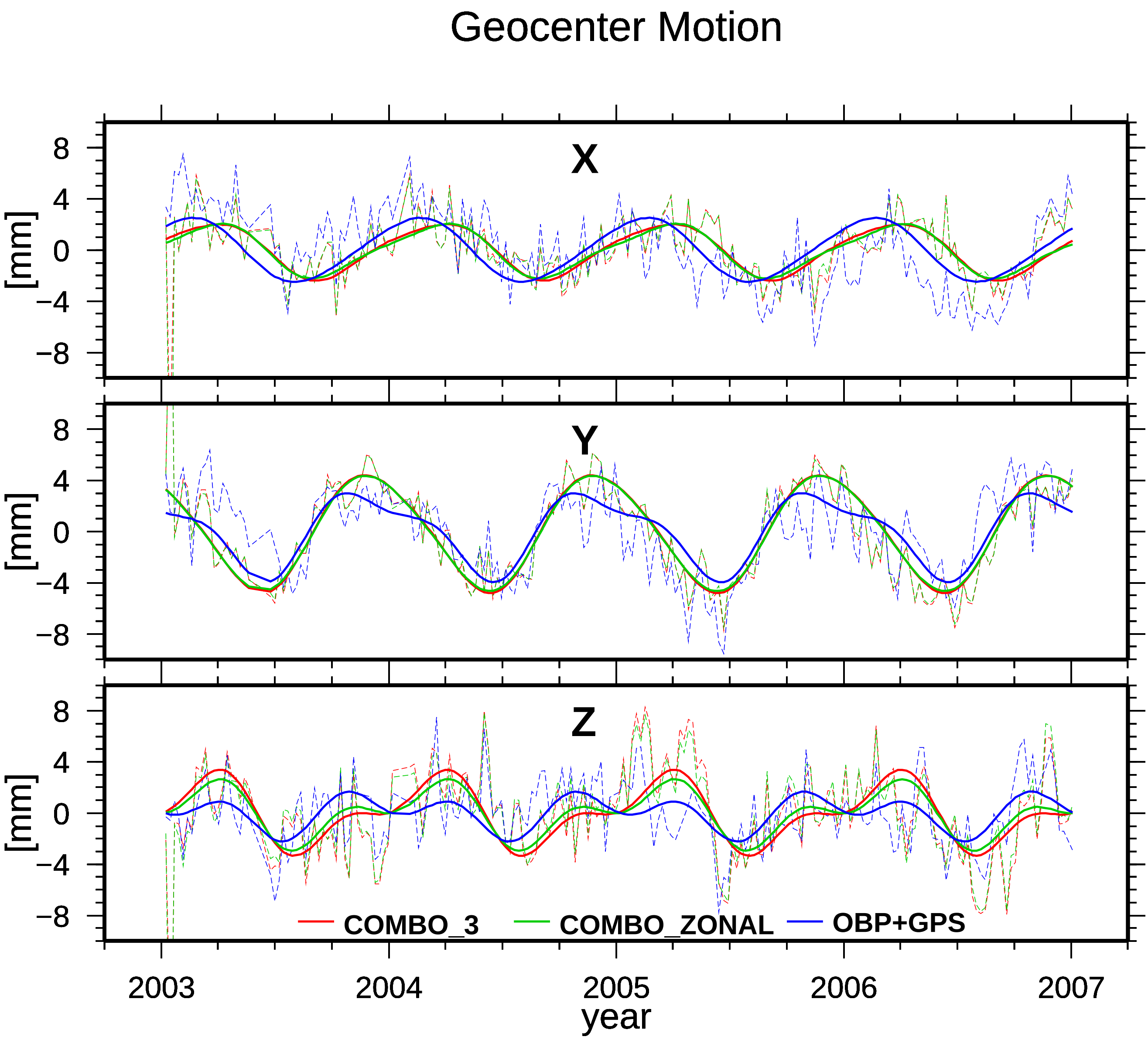

Figure 8. Estimated geocenter motion (CE wrt. the CM) in [mm] for three weighting scenarios. Combination with global FESOM coverage (with $\sigma = 3cmand4.8cm$ (red and blue resp.), and the combination with FESOM for $|lat| \leq 72.5°$ (green). The thick lines indicate a annual + semi annual fitted curve.

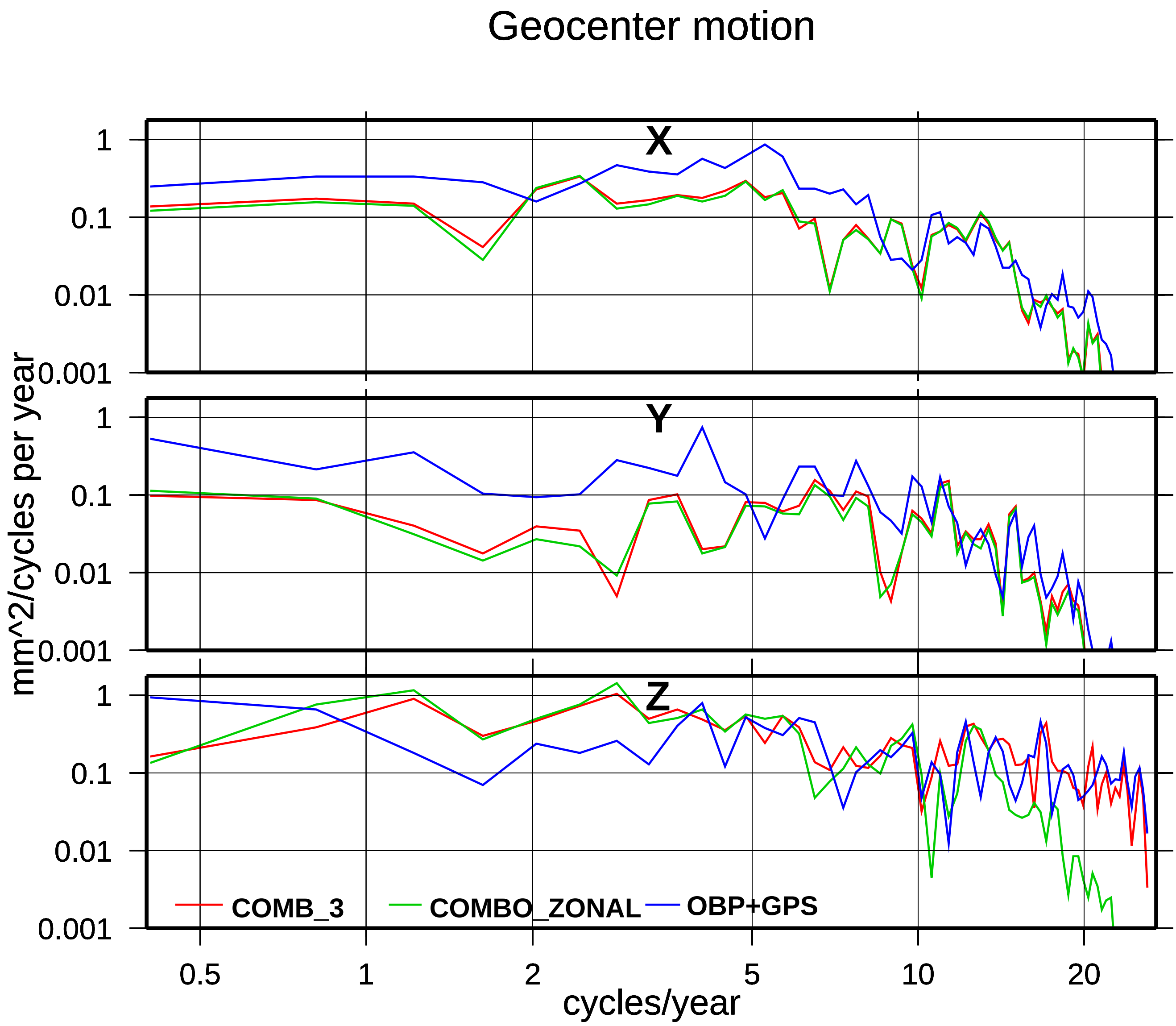

Figure 9. Power spectral density of the non-seasonal estimated geocenter motion (CE wrt. the CM) for the two weighting scenarios. Combination with global FESOM coverage (red) versus the combination with FESOM for $|lat| \leq 72.5°$.

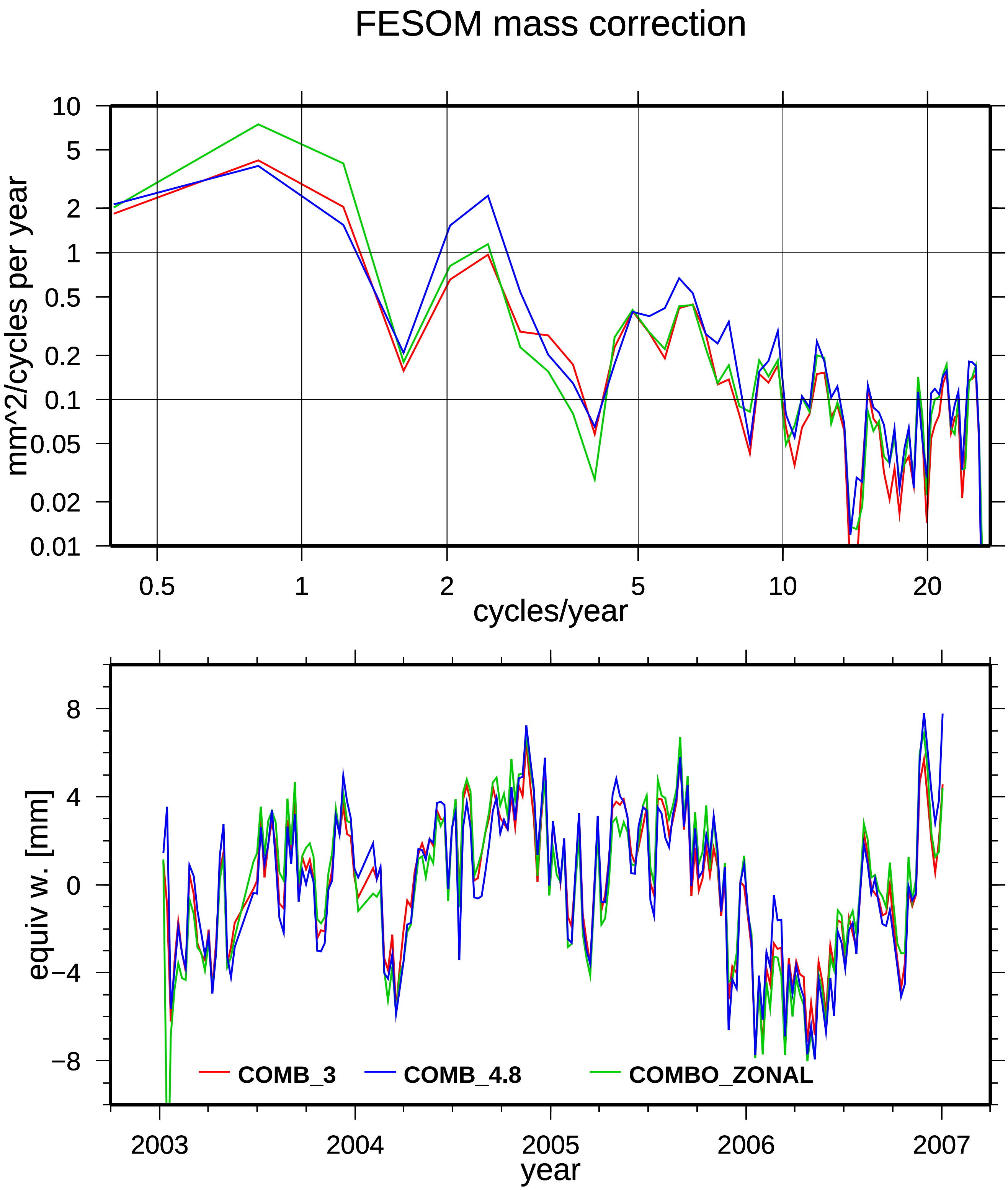

Figure 10. Power spectral density (top) and time series of oceanic mass correction estimated from the three combination schemes (red:FESOM, blue: FESOM $|lat| \leq 72.5°$ and green:cosine latitude weighted FESOM).

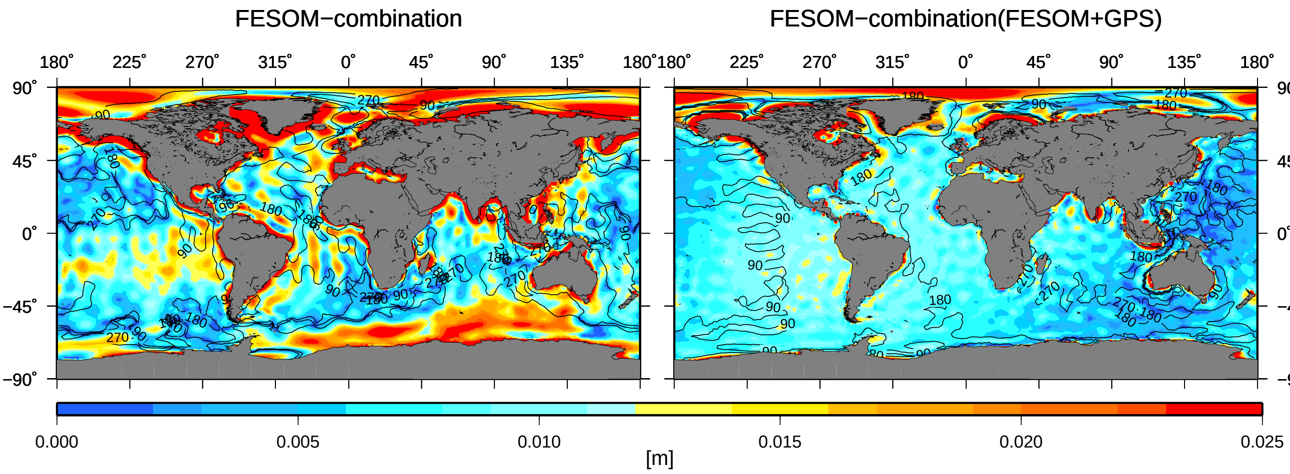

Figure 11. Annual amplitude (colors) and phase (contours in day of maximum) of bottom pressure differences between FESOM and the combination solution (equivalent water height in [m]). Left: Full combination, Right: combination with FESOM and GPS only.

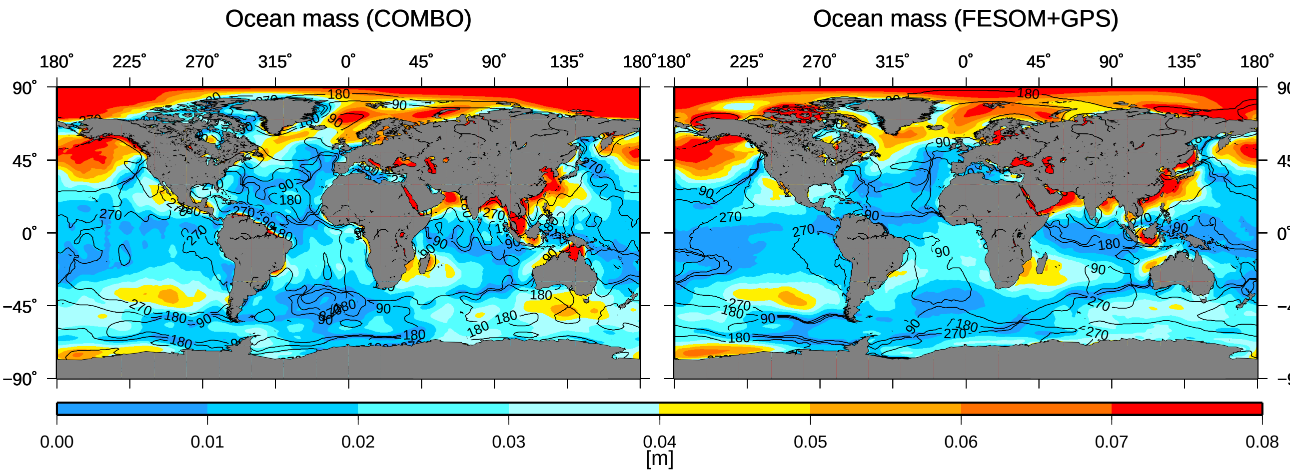

Figure 12. Annual amplitude (colors) and phase (contours in day of maximum) of ocean mass variations (OBP minus GAA) in equivalent water height. Left: Full combination, Right: combination with FESOM and GPS only.

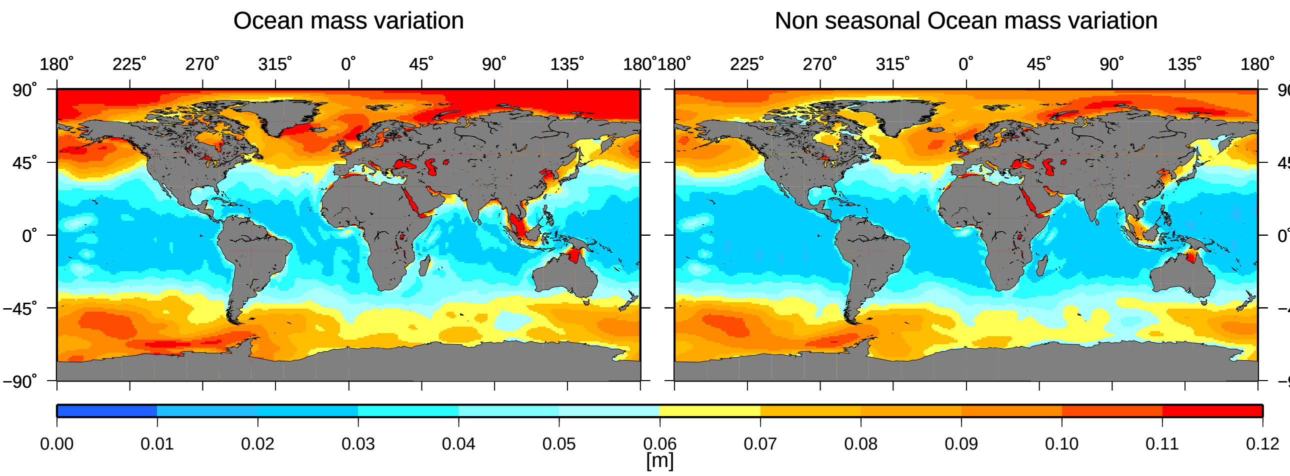

Figure 13. Left: RMS variability of ocean mass (OBP minus GAA product) in equivalent water height in [m]. Right: The same but with the seasonal cycles (annual+semiannual) removed.

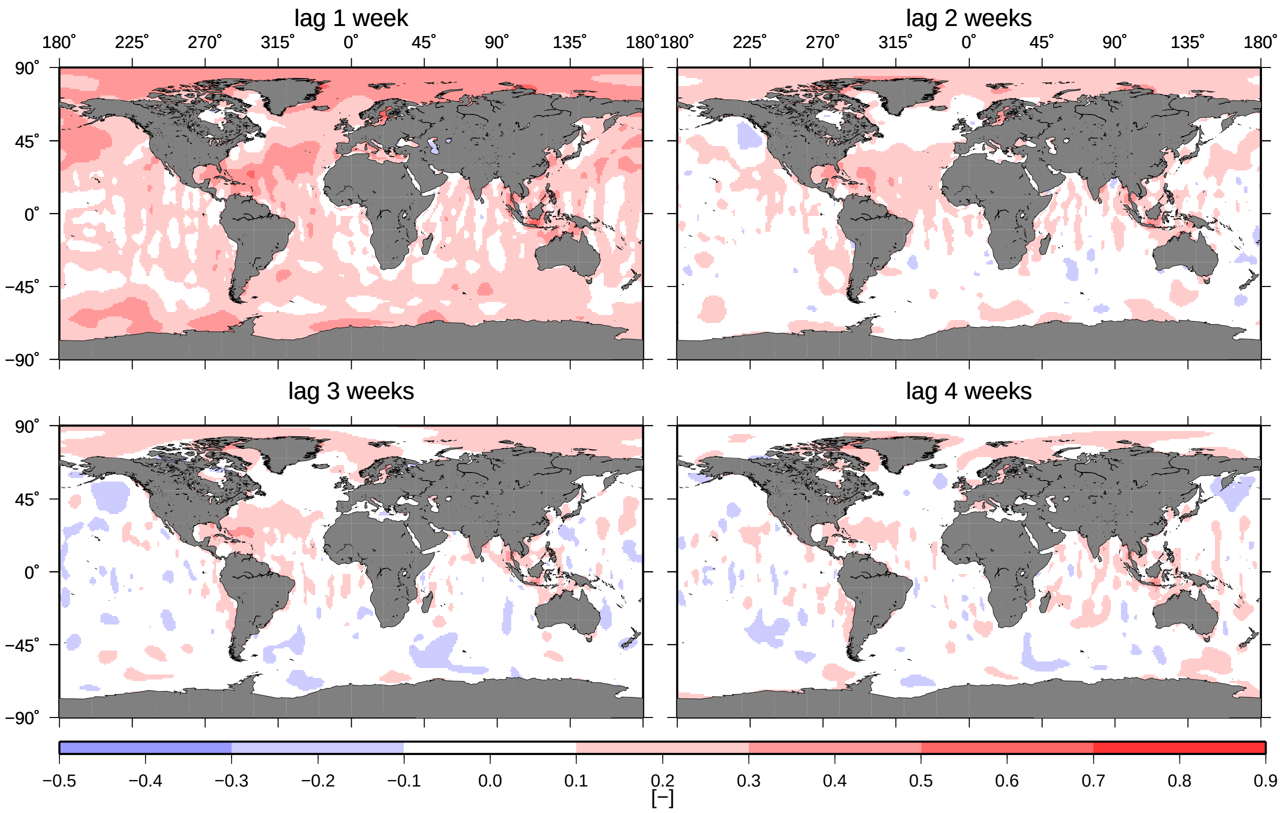

Figure 14. Short-term autocorrelation of ocean mass change (OBP minus GAA product), annual signal removed. Top left: for lag 1 week. Top right: for lag 2 weeks. Bottom left: for lag 3 weeks. Bottom right: for lag 4 weeks.

Location/BPR		COMBO			FESOM			GRACE wkly		
	RMS	corr	RMS	diffRMS	corr	RMS	diffRMS	corr	RMS	diffRMS
Crozet	3.1	0.7	2.8	2.2	0.6	1.6	2.5	0.5	3.6	3.4
Kerguelen	2.8	0.7	2.9	2.0	0.8	1.5	1.8	0.4	3.6	3.6
Mid Croz-Kerg	2.6	0.8	2.9	1.8	0.7	1.4	1.9	0.5	3.6	3.4

Table 1. Correlations of the weekly time series derived from in situ pressure records with time series of the combination solutions, FESOM and a GRACE only weekly solution. The first 5 weeks of the BPR records are ignored to prevent contamination by instrumental drift. Furthermore, root mean squares (in cm) of the full and residual timeseries are also provided under RMS and diffRMS respectively.

author	method	time span	annual mass		phase
			[10^{15}kg]	[mm]	[DOY]
Blewitt and Clarke [2003]	ge[1]	1996-2001	2.9[6]	7.6[6,8]	237[6]
Chambers et al. [2004]	gr	2002-2004		8.4	270
Chambers et al. [2004]	al[7,9]	2002-2004		8.5	282
Kusche and Schrama [2005]	ge[2]	1999-2005	2.1[6]	(5.8)	251[6]
Wenzel and Schröter [2007]	mo	1993-2003	1.7	(4.6)	283
Willis et al. [2008]	gr	2003-2007		6.8	265
Wu et al. [2006]	gr,ge,mo	2002-2004		6.4,9.0[6]	288,238[6]
Wu et al. [2006]	ge,mo	2002-2004		3.9	285
Wu et al. [2006]	gr[4]	2002-2004		6.6	292
This study FESOM only	mo	2003-2007		9.0,11.2[6]	287,247[6]
This study GRACE only[10]	gr	2003-2007		6.4,6.1[6]	307,267[6]
This study (OBP $\sigma = 3$ cm)	gr,ge,mo	2003-2007		7.4,8.7[6]	295,247[6]
This study (OBP $\sigma = 4.8$ cm)	gr,ge,mo	2003-2007		7.2,8.8[6]	293,245[6]
This study (OBP $\lvert lat \rvert \leq 72.5°$)	gr,ge,mo	2003-2007		6.9,8.1[6]	298,246[6]

Table 2. Annual component of ocean mass change, from several sources and from this study. Methods: ge[ometry], gr[avity], al[timetry], mo[delling]. [1] L=1, constrained by sea-level equation ('passive ocean'). [2] L=7, total energy constrained over the ocean. [4] l=1 and c_{20} from GRACE+GPS+ECCO. [6] sum of atmosphere and ocean mass change. [7] covers ±66° latitude. [8] mean relative sea level found to 8.0mm. [9] no IB-correction applied. [10] No geocenter motion. Phase is given in peak time (in day of year) counted from 1 January.

author Annual component	method	time span	x-am [mm]	x-ph [DOY]	y-am [mm]	y-ph [DOY]	z-am [mm]	z-ph [DOY]
Swenson et al. [2008] ('GRACE-ECCO')	gr,mo	2003-2007	1.1	52	2.7	325	1.2	55
Swenson et al. [2008] ('GRACE-OMCT')	gr,mo	2003-2007	1.9	46	2.6	326	1.8	60
Moore and Wang [2003]	slr	1993-2001	3.5	26	4.3	303	4.6	33
Crétaux et al. [2002]	slr	1993-1999	2.6	32	2.5	309	3.3	36
Crétaux et al. [2002]	slr,do	1993-1999	1.1	16	3.7	292	3.0	57
Bouillé et al. [2000]	slr,do	1993-1997	2.1	48	2.0	327	3.5	43
Wu et al. [2006]	gr,ge,mo	2002-2004	1.8	46	2.5	329	3.9	28
This study (OBP $\sigma = 3$ cm)	gr,ge,mo	2003-2007	2.1	75	4.5	338	2.5	63
This study (OBP $\sigma = 4.8$ cm)	gr,ge,mo	2003-2007	2.1	71	4.4	338	2.4	58
This study (OBP $\|lat\| \leq 72.5°$)	gr,ge,mo	2003-2007	2.0	76	4.5	338	1.9	55
This study (OBP+GPS)	ge,mo	2003-2007	2.5	42	3.0	336	1.1	360
Semi annual Component								
Crétaux et al. [2002]	slr	1993-1999	1.0	132	0.4	95	1.0	62
Crétaux et al. [2002]	slr,do	1993-1999	2.6	32	2.5	309	3.3	36
Wu et al. [2006]	gr,ge,mo	2002-2004	0.6	121	1.3	143	0.8	110
This study (OBP $\sigma = 3$ cm)	gr,ge,mo	2003-2007	0.3	143	0.4	94	1.4	107
This study (OBP $\sigma = 4.8$ cm)	gr,ge,mo	2003-2007	0.3	143	0.4	93	1.4	112
This study(OBP $\|lat\| \leq 72.5°$)	gr,ge,mo	2003-2007	0.4	129	0.4	97	1.3	108
This study (OBP+GPS)	ge,mo	2003-2007	0.2	86	1.1	87	1.2	107

Table 3. Estimates of annual and semi annual geocenter motion, from several sources and from this study. 'do' denote DORIS measurements.